

1 **Formaldehyde distribution over North America: Implications for**
2 **satellite retrievals of formaldehyde columns and isoprene emission**

3
4
5
6 **Dylan B. Millet, Daniel J. Jacob, Solène Turquety, Rynda C. Hudman, and Shiliang Wu**

7 Department of Earth and Planetary Sciences and Division of Engineering and Applied Sciences,
8 Harvard University, Cambridge, Massachusetts, USA
9

10 **Alan Fried and James Walega**

11 Earth Observing Laboratory, National Center for Atmospheric Research, Boulder, Colorado,
12 USA
13

14 **Brian G. Heikes**

15 Graduate School of Oceanography, University of Rhode Island, Narragansett, Rhode Island,
16 USA
17

18 **Donald R. Blake**

19 Department of Chemistry, University of California, Irvine, California, USA
20

21 **Hanwant B. Singh**

22 NASA Ames Research Center, Moffett Field, California, USA
23

24 **Bruce E. Anderson**

25 Atmospheric Sciences Division, NASA Langley Research Center, Hampton, Virginia, USA
26

27 **Antony D. Clarke**

28 School of Ocean and Earth Science and Technology, University of Hawaii at Manoa, Honolulu,
29 Hawaii, USA
30
31
32

33 **Short title:** Formaldehyde over North America

34 **Submitted to:** Journal of Geophysical Research – Atmospheres
35 November 4, 2005

36 **Index terms:** 0315, 0322, 0345, 0365, 0394

37 **Author keywords:** Formaldehyde, isoprene, satellite, aircraft, GOME, OMI

Abstract.

Formaldehyde (HCHO) columns measured from space provide constraints on emissions of volatile organic compounds (VOCs). Quantitative interpretation requires characterization of errors in HCHO column retrievals and relating these columns to VOC emissions. Retrieval error is mainly in the air mass factor (AMF) which relates fitted backscattered radiances to vertical columns, and requires external information on HCHO, aerosols, and clouds. Here we use aircraft data collected over North America and the Atlantic to determine the local relationships between HCHO columns and VOC emissions, calculate AMFs for HCHO retrievals, assess the errors in deriving AMFs with a chemical transport model (GEOS-Chem), and draw conclusions regarding space-based mapping of VOC emissions. We show that isoprene drives observed HCHO column variability over North America; HCHO column data from space can thus be used effectively as a proxy for isoprene emission. From observed HCHO and isoprene profiles we find an HCHO molar yield from isoprene oxidation of 1.6 ± 0.5 , consistent with current chemical mechanisms. Clouds are the primary error source in the AMF calculation; errors in the HCHO vertical profile and aerosols have comparatively little effect. The mean bias and 1σ uncertainty in the GEOS-Chem AMF calculation increase from $<1\%$ and 15% for clear skies to 17% and 24% for half-cloudy scenes. With fitting errors, this gives an overall 1σ error in HCHO satellite measurements of $25\text{--}31\%$. Retrieval errors, combined with uncertainties in the HCHO yield from isoprene oxidation, result in a 40% (1σ) error in inferring isoprene emissions from HCHO satellite measurements.

1. Introduction

Atmospheric volatile organic compounds (VOCs) are precursors of tropospheric ozone and secondary organic aerosol, and play an important role in HO_x and NO_y radical cycling. Bottom-up VOC emission estimates, relying on extrapolation of point measurements to regional and larger scales, are inherently uncertain. Formaldehyde (HCHO), which is produced in high yield during the atmospheric oxidation of VOCs, absorbs in the near-UV and can be measured as a column integral from satellite-borne solar backscatter instruments [Burrows *et al.*, 1999; Chance *et al.*, 2000]. Such measurements offer the means to derive global, top-down constraints on surface emissions of VOCs. In order to do so reliably we need to quantify the errors associated with the column measurements and their relationship to precursor emissions. Here we use aircraft vertical profiles over North America collected during the Intercontinental Chemical Transport Experiment (INTEX-A) aircraft campaign in summer 2004 [Singh *et al.*, 2006] to quantify the dominant errors in satellite retrievals of HCHO columns, and determine how the HCHO column and its variability can be interpreted in terms of the underlying reactive VOC emissions.

While oxidation of methane is the main HCHO source in the remote atmosphere [Lowe and Schmidt, 1983; Singh *et al.*, 2000; Heikes *et al.*, 2001; Frost *et al.*, 2002; Wagner *et al.*, 2002], more reactive VOCs frequently dominate in the continental boundary layer [Lee *et al.*, 1998; Fried *et al.*, 2003]. The main HCHO sinks are reaction with the hydroxyl radical and photolysis [Levy, 1972], which combine to give an atmospheric lifetime of a few hours in daytime [Atkinson, 2000].

Isoprene, a highly reactive compound which is the principal VOC emitted from vegetation [Zimmerman *et al.*, 1978; Fehsenfeld *et al.*, 1992; Fuentes *et al.*, 2000; Guenther *et al.*, 2000], is

1 in particular a major source of HCHO during the growing season [Zimmerman *et al.*, 1978;
2 Hanst *et al.*, 1980; Shepson *et al.*, 1991; Lee *et al.*, 1998]. Globally, emissions of isoprene are
3 estimated to be around 500 Tg yr⁻¹ [Guenther *et al.*, 1995; Wang and Shallcross, 2000; Potter *et*
4 *al.*, 2001; Levis *et al.*, 2003; Sanderson *et al.*, 2003; Naik *et al.*, 2004; Guenther *et al.*, 2006],
5 substantially greater than the total VOC emissions from all anthropogenic sources [Singh and
6 Zimmerman, 1992]. Even over densely populated and industrialized eastern North America, on
7 regional scales isoprene far exceeds anthropogenic VOC emissions during the growing season
8 [Jacob *et al.*, 1993] and is a major source of surface ozone [Fiore *et al.*, 2005] and also possibly
9 organic aerosol [Jang *et al.*, 2002; Czoschke *et al.*, 2003; Limbeck *et al.*, 2003; Claeys *et al.*,
10 2004a; Claeys *et al.*, 2004b; Zhang *et al.*, 2004; Lim *et al.*, 2005].

11 Despite considerable efforts in constructing bottom-up emission inventories for isoprene and
12 other biogenic VOCs, important uncertainties remain because of the need to extrapolate over
13 vegetation types, the complex effects of environmental stressors, and evolving land cover
14 [Guenther *et al.*, 2000]. Palmer *et al.* [2001; 2003] developed a top-down approach for inferring
15 isoprene emission fluxes using space-based column measurements of HCHO, and applied it to
16 derive emissions from North America using data from the Global Ozone Monitoring Experiment
17 (GOME) satellite instrument. This work has since been extended to examine seasonal and
18 interannual variability in North American isoprene emissions [Abbot *et al.*, 2003; Palmer *et al.*,
19 2006]. Recently, [Shim *et al.*, 2005] carried out a Bayesian inversion of GOME HCHO column
20 measurements for different continental source regions, and derived global isoprene emissions
21 50% larger than the a priori estimate.

22 Work to date in this area has used data from GOME, which has 40 km x 320 km resolution
23 and global coverage every three days. The Ozone Monitoring Instrument (OMI), which was

launched in 2004 aboard the NASA Aura satellite, provides daily global coverage and a footprint of 13 x 24 km. HCHO columns measured from OMI should enable us to quantify surface fluxes of VOCs at a far greater level of temporal and spatial detail than is possible with GOME. The validity of such analyses depends on the uncertainties associated with the retrieval of HCHO vertical columns from the satellite spectra and with their interpretation in terms of VOC emission. The dominant source of error in the retrieval is the air mass factor (AMF) [Palmer *et al.*, 2006], which defines the relationship between the HCHO abundance along the viewing path of the satellite instrument (“slant column”) and the vertical column amount [Noxon *et al.*, 1979; Perliski and Solomon, 1993; Marquard *et al.*, 2000; Palmer *et al.*, 2001; Hild *et al.*, 2002; Richter and Burrows, 2002; Boersma *et al.*, 2004]. The AMF calculation requires external information on atmospheric scattering by air molecules, clouds and aerosols, on the shape of the HCHO vertical distribution, and on the UV albedo of the surface. Clouds, which increase instrument sensitivity to the absorber above the cloud while decreasing it below, represent a significant source of uncertainty in the computation of the AMF [Koelemeijer and Stammes, 1999; Velders *et al.*, 2001; Richter and Burrows, 2002; Martin *et al.*, 2003a; Boersma *et al.*, 2004]. The interpretation of observed HCHO columns in terms of precursor VOC emissions also requires prior information on the relationship between the VOC surface flux and the resulting HCHO column amount.

INTEX-A included numerous aircraft profiles over North America. The resulting dataset, which includes measurements of HCHO together with VOCs, aerosol extinction, and cloud extinction, provides us with an excellent opportunity to go beyond previous work and address this issue. In the present study, we use the INTEX-A aircraft data and output from the GEOS-Chem chemical transport model (CTM) to: 1) determine the important precursors contributing to

HCHO columns and variability over North America, and quantify the relationships between precursor emissions and HCHO columns; 2) carry out a statistically meaningful and geographically extensive quantification of the errors in the AMF calculation; and 3) draw conclusions regarding the mapping of VOC emissions from space.

2. Background

2.1. Satellite Retrievals of HCHO Columns

The retrieval of atmospheric HCHO column abundance using space-borne solar backscatter instruments can be performed by fitting the backscattered spectrum in the HCHO absorption window (337 – 356 nm) to modeled atmospheric spectra (e.g., [Chance *et al.*, 2000]), or by differential optical absorption spectroscopy (e.g., [Leue *et al.*, 2001]). The resulting HCHO abundance integrated along the viewing path is called the slant column, and the ratio of the slant column to the actual vertical column is termed the AMF. In the case of a non-scattering atmosphere, the geometric air mass factor AMF_G would be determined solely by the satellite viewing angle (θ_V) and the solar zenith angle (θ_S):

$$AMF_G = \sec \theta_S + \sec \theta_V . \quad (1)$$

This simple expression must be corrected for scattering by air molecules, clouds, and aerosols, which results in sensitivity to the vertical distribution of the absorbing gas and to the surface albedo. The correction factor can be expressed in the optically thin case as an integral of sensitivity over the depth of the atmosphere [Palmer *et al.*, 2001]:

$$AMF = \frac{AMF_G}{P_S} \int_{P_S}^0 w(P) \mathcal{S}(P) dP , \quad (2)$$

1 where P is pressure and P_s is the pressure at Earth's surface. The scattering weights $w(P)$
2 represent the sensitivity of the backscattered radiation measured from space to the abundance of
3 the absorber (here HCHO) at pressure P , and are determined using a radiative transfer model.
4 The shape factor $S(P)$ is the normalized vertical profile of mixing ratio of the absorber, and is
5 determined from typical atmospheric observations or an atmospheric CTM. Aerosol vertical
6 profiles for the radiative transfer calculation are similarly specified from climatologies [*Velders*
7 *et al.*, 2001; *Richter and Burrows*, 2002; *Beirle et al.*, 2004a; *Richter et al.*, 2004; *Savage et al.*,
8 2004], or from the same CTM used to specify $S(P)$ [*Martin et al.*, 2003a; *Jaeglé et al.*, 2004].
9 Like clouds, aerosols can act to either increase or decrease the instrument sensitivity to HCHO,
10 depending on the single scattering albedo of the aerosol and its vertical distribution relative to the
11 absorber.

12 Satellite viewing scenes are typically partly cloudy, particularly for an instrument with a
13 large footprint such as GOME. The ability to resolve partly cloudy scenes in the retrieval is thus
14 critical to the data coverage. In the case of GOME, broadband polarization monitoring devices
15 provide information on cloud fraction, and spectral fitting in and around the oxygen A-band
16 provides information on cloud top altitude and cloud optical depth [*Kurosu et al.*, 1999;
17 *Koelemeijer et al.*, 2001]. Previous GOME retrievals for HCHO or NO₂ have either assumed
18 cloud effects to be negligible for pixels having cloud fractions below a given threshold [*Palmer*
19 *et al.*, 2001; *Lauer et al.*, 2002; *Richter and Burrows*, 2002; *Ladstatter-Weissenmayer et al.*,
20 2003; *Palmer et al.*, 2003; *Stohl et al.*, 2003; *Beirle et al.*, 2004a; *Richter et al.*, 2004; *Savage et*
21 *al.*, 2004; *Irie et al.*, 2005; *Konovalov et al.*, 2005], applied a constant correction factor to cloudy
22 scenes [*Leue et al.*, 2001; *Velders et al.*, 2001; *Beirle et al.*, 2003], or calculated the radiative

transfer through clouds explicitly using local cloud information [*Martin et al.*, 2002a; *Abbot et al.*, 2003; *Martin et al.*, 2003a; *Jaeglé et al.*, 2004; *Palmer et al.*, 2006].

In the latter approach, developed by *Martin et al.* [2002a], the AMF for a partly cloudy scene is derived as the weighted sum of the values for the clear and cloudy subscenes:

$$\text{AMF} = \frac{\text{AMF}_{\text{clear}} R_{\text{clear}} (1 - f) + \text{AMF}_{\text{cloud}} R_{\text{cloud}} f}{R_{\text{clear}} (1 - f) + R_{\text{cloud}} f}, \quad (3)$$

where f is the cloud fraction, and R_{clear} and R_{cloud} are the reflectivities of the clear and cloudy portions of the retrieval scene. The two subscenes are assumed to have the same HCHO shape factor $S(P)$. *Martin et al.* [2002a] and the subsequent studies calculated the AMF for the cloudy subscene by using the GOME information on cloud top and optical depth, and distributing the cloud extinction vertically assuming an optical thickness increment of 8 for each 100 hPa below cloud top.

The primary uncertainties in space-borne measurements of HCHO columns arise from the slant column fitting [*Chance et al.*, 2000], which defines the instrumental detection limit, and errors in the AMF, which define a relative error for columns well above the detection limit [*Palmer et al.*, 2001; *Martin et al.*, 2002a; *Boersma et al.*, 2004; *Palmer et al.*, 2006]. The slant column fitting uncertainty is 4×10^{15} molecules cm^{-2} for GOME. The main sources of error in the AMF are the surface albedo, specification of the HCHO vertical profile, and aerosol and cloud effects, and quantification of this error is a focus of our paper.

2.2. Relating HCHO Columns to Precursor Emissions

Column HCHO measurements from space can be used to derive precursor emission fluxes [*Palmer et al.*, 2003], provided the associated HCHO production yields are known. At steady

state and in the absence of horizontal transport, the HCHO column (Ω_{HCHO} , molecules cm^{-2}) would be related to the emissions of precursors i by

$$\dot{\Omega}_{\text{HCHO}} = \frac{1}{k_{\text{HCHO}}} \sum_i k_i Y_i \dot{\Omega}_i = \frac{1}{k_{\text{HCHO}}} \sum_i Y_i E_i, \quad (4)$$

where k_{HCHO} and k_i are the column-average effective rate constants (s^{-1}) for chemical loss of HCHO and precursor i , Y_i is the molar HCHO yield from the oxidation of species i , and E_i is the emission flux. Horizontal transport smears this relationship, resulting in a spatial offset between the HCHO column and the location of precursor emission, and diluting the HCHO signal associated with the emission [Palmer *et al.*, 2003]. For isoprene, which has a lifetime in summer of ~ 0.5 h and yields HCHO in its first generation of products, the smearing length scale is only 10-100 km, smaller than the GOME pixel size [Palmer *et al.*, 2003]. For longer-lived VOCs or VOCs with delayed HCHO production, the smearing length scale may be sufficiently large to dilute the HCHO signal to below the fitting uncertainty [Palmer *et al.*, 2006]. This smearing effect will limit gains in spatial resolution otherwise achievable with new satellite instruments unless other techniques are developed.

Inferring VOC emission fluxes from observed HCHO columns requires assumptions about the HCHO yield Y_i . Palmer *et al.* [2006] computed the time-dependent HCHO yield from isoprene oxidation using two independent mechanisms, GEOS-Chem (<http://www-as.harvard.edu/chemistry/trop/geos/index.html>) and the Master Chemical Mechanism (MCM) v. 3.1 [Bloss *et al.*, 2005]. They found the yield calculated by MCM to be 20-30% higher than that derived by GEOS-Chem. The resulting HCHO molar yields after one day under low- NO_x (0.1 ppb) conditions are 0.9 (GEOS-Chem) and 1.6 (MCM). The high- NO_x (1 ppb) molar yields are 1.9 (GEOS-Chem) and 2.4 (MCM).

3. Approach

The previous section has highlighted a number of uncertainties in the derivation of VOC emissions from space-based HCHO column measurements. In this section we describe our use of the INTEX-A aircraft measurements to better quantify these uncertainties and thus improve the constraints on the top-down VOC emission estimates. We use the GEOS-Chem CTM as the source of external information here but our findings can be applied to any CTM-assisted retrieval.

3.1. Measurements

The primary objective of INTEX-A (July 1 – August 15, 2004) was to observe the chemical outflow from North America and infer constraints on chemical sources and export. Here we use measurements of HCHO and related tracers made aboard the NASA DC-8 aircraft (ceiling 12 km) over North America and the adjacent oceans during INTEX-A. The DC-8 aircraft flew 18 science flights between July 1 and August 15 with extensive vertical profiling from the boundary layer to the upper troposphere. All flights took place during daytime, typically from 10:00 to 18:00 local time. The flight tracks are shown in Figure 1.

HCHO measurements were carried out by two groups, from the National Center for Atmospheric Research (NCAR) and the University of Rhode Island (URI) (hereafter referred to as the NCAR and URI measurements, respectively). HCHO was measured by the NCAR group using tunable diode laser absorption spectroscopy [*Wert et al.*, 2003; *Fried et al.*, 2006; *Roller et al.*, 2006]. The total calibration uncertainty is estimated to be $\pm 12\%$ (2σ), and the limit of detection (LOD) is 77 ppt for the first part of the mission and 66 ppt for the last 7 flights

(07/31/2004 – 08/14/2004), for 1-minute averaged data (both 2σ). The measurement precision is the same as the LOD over the HCHO mixing ratios measured during INTEX-A. The URI HCHO measurement was performed using aqueous collection and enzyme-fluorescence detection [Heikes *et al.*, 2001]. The LOD is 50 ppt for the first part of the mission, and 25 ppt for the last 5 flights (08/06/2004 – 08/14/2004). The total uncertainty in the measurement is estimated at $\pm (33 \text{ ppt} + 0.15*[\text{HCHO mixing ratio}])$. Measurements from the two groups were highly correlated over the ensemble of the INTEX-A mission ($R^2 = 0.89$). However, a reduced major axis regression of the two datasets yields a slope of 0.69, with the URI data being lower than the NCAR data. A detailed measurement intercomparison will be presented elsewhere [Fried *et al.*, 2006].

Oxygenated VOCs were measured with a sampling frequency of 2.5 – 5 minutes using cryogenic preconcentration, gas chromatographic (GC) separation and detection by photoionization detector and reduction gas detector [Singh *et al.*, 2004]. Detection limits range from 5 – 20 ppt, and the sensitivity and precision of measurement are approximately 20% and 10%. Hydrocarbons were measured by whole air sampling followed by cryogenic preconcentration, GC separation and detection by flame ionization detector and mass selective detector [Colman *et al.*, 2001; Blake *et al.*, 2003]. Calibration was based on whole air standards (for $<C_8$ gases) and per-carbon response factors (for C_8 - C_{10} gases). The limit of detection is approximately 3 ppt for the species reported here. The measurement precision and overall accuracy are 1-3% and 2-10% respectively, depending on the compound.

Aerosol scattering coefficients were measured at 450, 550, and 700 nm using two TSI 3563 3-wavelength integrating nephelometers. The value at 346 nm was estimated from the Angstrom exponent derived from the 450 nm and 550 nm measurements. Aerosol absorption coefficients

at 470, 530 and 660 nm were measured using a pair of Radiance Research Particle Soot Absorption Photometers [Bond *et al.*, 1999; Virkkula *et al.*, 2005]; the absorption coefficient at 346 nm was assumed equal to that at 470 nm.

3.2. Model Description

Atmospheric distributions of HCHO and related tracers were simulated for the INTEX-A period using the GEOS-Chem global 3D CTM [Bey *et al.*, 2001; Park *et al.*, 2004]. The GEOS-Chem CTM (version 7.02, <http://www-as.harvard.edu/chemistry/trop/geos/index.html>) uses GEOS-4 assimilated meteorological data from the NASA Goddard Earth Observing System including winds, convective mass fluxes, mixing depths, temperature, precipitation, and surface properties. The data have 6-hour temporal resolution (3-hour for surface variables and mixing depths), $1^\circ \times 1^\circ$ horizontal resolution, and 48 sigma vertical layers. We degrade the horizontal resolution to $2^\circ \times 2.5^\circ$ for input to GEOS-Chem.

The model includes detailed ozone-NO_x-VOC chemistry coupled to aerosols. Global emissions are as described by [Bey *et al.*, 2001], with recent updates [Martin *et al.*, 2002b; Park *et al.*, 2004; Xiao *et al.*, 2004]. Isoprene emissions are calculated using the GEIA inventory [Guenther *et al.*, 1995]. Anthropogenic emissions from North America are based on the EPA NEI 1999 v.1 inventory (<http://www.epa.gov/ttn/chief/net/1999inventory.html>). The aerosol simulation is as described by [Park *et al.*, 2003; Park *et al.*, 2004], and includes sulfate-nitrate-ammonium, organic and black carbon, size-resolved soil dust, and size-resolved sea salt. Aerosol optical thicknesses are calculated from the mass concentrations and optical properties for each aerosol type, as a function of local relative humidity, following [Martin *et al.*, 2003b]. Previous studies have compared GEOS-Chem results with observations over North America and

the North Atlantic for HCHO [*Singh et al.*, 2000; *Palmer et al.*, 2001; *Fiore et al.*, 2002; *Martin et al.*, 2004] and aerosols [*Park et al.*, 2003; *Park et al.*, 2004; *van Donkelaar et al.*, 2006]. The current simulation was conducted at $2^{\circ} \times 2.5^{\circ}$ horizontal resolution and with 30 vertical layers. Results are presented here for July and August 2004, and follow a one year spinup.

Applications of GEOS-Chem to simulation of other aspects of INTEX-A data include analyses of North American NO_x emissions and reactive nitrogen export [*Hudman et al.*, 2006], boreal fire emissions [*Turquety et al.*, 2006], Asian inflow [*Liang et al.*, 2006], and the upper tropospheric ozone budget [*Li*, 2006].

4. Atmospheric Distribution of HCHO over North America

4.1. Vertical Distributions

Mean observed and simulated vertical distributions of HCHO are displayed in Figure 2, for the ensemble of the data, as well as continental and oceanic subsets. Here and elsewhere, the model is sampled along the flight tracks and for the times of the measurements. Mixing ratios are high in the continental boundary layer due to surface emissions of HCHO precursors, and decrease rapidly with altitude because of the short HCHO lifetime. Mixing ratios over the ocean are lower and decrease more gradually with altitude, reflecting primarily the temperature dependence of methane oxidation. Observed continental mixing ratios decrease from a mean of 1800 ppt (URI) – 2700 ppt (NCAR) near the surface to 230 ppt (URI) – 420 ppt (NCAR) at 550 hPa, and continue to decrease at higher altitudes. However, elevated HCHO mixing ratios were observed on numerous occasions at altitudes above 6 km over the eastern United States due to convection of boundary layer precursors; this will be discussed in more detail by *Fried et al.* [2006]. Over the ocean, HCHO concentrations decrease from 540 ppt (URI) - 880 ppt (NCAR)

near the surface to 120 ppt (URI) – 230 ppt (NCAR) at 550 hPa. The 30% offset between the NCAR and URI measurements is evident in the mean vertical distributions (Figure 2); for both the continental and oceanic subsets, the simulated mixing ratios fall within the range defined by the two sets of observations. The relative vertical distribution (shape factor), critical for our application, is also well simulated. Over the continent, measured and modeled ratios of the mean HCHO concentration at 960 vs. 550 hPa are 6.3 (NCAR), 8.0 (URI) and 7.8 (GEOS-Chem). The corresponding values over the ocean are 3.8 (NCAR), 4.3 (URI) and 3.7 (GEOS-Chem). Further analysis of shape factors in the context of the AMF calculation will be discussed below.

4.2. Vertical Columns

We calculated HCHO vertical columns from observed and simulated HCHO mixing ratios during the DC-8 vertical profiles. Extensive vertical profiling from the boundary layer (~300 m above surface) to the upper troposphere (~10 km) was conducted during the mission. Here, we define as a vertical profile any flight segment meeting the following criteria: 1) observations extending from below 600 m (1000 m for marine profiles) to above 8 km radar altitude, 2) horizontal drift of less than 3° latitude x 4° longitude, and 3) at least 15 valid measurements. Mixing ratios above and below the profile were estimated by extending the values obtained at the highest and lowest altitudes uniformly to the tropopause and to Earth's surface. Mixing ratios in the stratosphere are negligible. Modeled columns calculated with these assumptions agree well with the corresponding model calculations for the full columns (slope = 0.97, $R^2 = 0.96$). We obtain in this manner 69 total profiles with a mean horizontal drift of ~190 km. Missing observations reduce the number of profiles to 36 for the NCAR HCHO dataset and 13 for the URI HCHO dataset.

Figure 3 shows the resulting HCHO columns. Measured values range from $0.4 - 3.1 \times 10^{16}$ molecules cm^{-2} over continental North America, and from $0.4 - 0.8 \times 10^{16}$ molecules cm^{-2} over the ocean. Again, the bias between the two sets of measurements is manifest. Both modeled and measured columns are highest over the southeast United States, reflecting elevated isoprene emission [Lee *et al.*, 1998] as discussed previously by Palmer *et al.* [2003]. Prior in situ observations have been too sparse to clearly define this maximum, but it is clearly revealed by the INTEX-A data. Scatterplots of simulated vs. observed HCHO vertical columns are displayed in Figure 4. The model captures 70% of the variability in the observed NCAR columns, and 42% of that in the URI columns. The modeled HCHO columns have a bias (given by the slope of the regression line) of +4% compared to NCAR and +34% compared to URI.

5. Relating HCHO Columns to reactive VOC emissions

In the following sections we use the data from the INTEX-A aircraft profiles to determine how column HCHO data from space can be interpreted in terms of the underlying reactive VOC emissions. Our first step is to determine which parent VOCs drive the variability in the HCHO column. For this purpose, we compute column integrated HCHO production rates from the precursor VOCs measured aboard the aircraft and relate those to the measured HCHO columns. Here and for the remainder of the paper we restrict our analysis to the NCAR HCHO dataset owing to its factor of ~ 2 higher data coverage.

HCHO yields (high- NO_x conditions) for all measured precursor VOCs with significant emissions are shown in Table 1. Yields and rates are obtained from the GEOS-Chem chemical mechanism, except where noted, and represent cumulative yields from the successive stages of

1 oxidation of the parent compound until a product with a lifetime longer than a few hours is
2 reached. The dependence of HCHO yields on NO_x is discussed by *Palmer et al.* [2003, 2006];
3 low- NO_x conditions leading to organic peroxide formation have little effect on ultimate yields if
4 the organic peroxides decompose to regenerate radicals, as is commonly assumed, but the HCHO
5 production is delayed.

6 Column integrated HCHO production rates (P_{HCHO} , molecules $\text{cm}^{-2} \text{ s}^{-1}$) from VOC oxidation
7 by OH were computed from the DC-8 vertical profiles for different classes of measured
8 precursors using rate constant data from [*Sander et al.*, 2002; *Atkinson et al.*, 2004], HCHO
9 yields from Table 1, and local OH concentrations from the GEOS-Chem model [*Hudman et al.*,
10 2006]. VOC vertical profiles were extrapolated below and above the aircraft in the same way as
11 HCHO. Results for isoprene, oxygenated volatile organic compounds (OVOCs), anthropogenic
12 non-methane organic compounds (ANMHC), the monoterpenes α - and β -pinene, and methane
13 are displayed as probability density functions in Figure 5. The slant column fitting error for the
14 satellite instrument (4×10^{15} molecules cm^{-2} for GOME [*Chance et al.*, 2000]), divided by the
15 HCHO column lifetime (~ 2 hours), gives a lower limit for the magnitude of the HCHO source
16 that can be detected from space ($\sim 0.6 \times 10^{12}$ molecules $\text{cm}^{-2} \text{ s}^{-1}$). Methane and the OVOCs are
17 ubiquitous in the atmosphere, and account for the majority of the total HCHO production.
18 However, the variability in the resulting HCHO production is low (standard deviations of 0.3 and
19 0.2×10^{12} molecules $\text{cm}^{-2} \text{ s}^{-1}$), and the column integrated HCHO production rate is always less
20 than twice the nominal satellite detection limit of 0.6×10^{12} molecules $\text{cm}^{-2} \text{ s}^{-1}$. These compounds
21 therefore give rise to a relatively stable HCHO column background over the study domain.
22 ANMHCs and monoterpenes are negligible under all conditions encountered during the vertical

1 profiles. Column HCHO production from isoprene, on the other hand, with a variability
2 (standard deviation 2.3×10^{12} molecules $\text{cm}^{-2} \text{s}^{-1}$) more than a factor of five greater than that due
3 to any other VOC group, reaches levels well above the minimum level detectable from space. We
4 conclude therefore that detectable variability in the HCHO column over North America in
5 summer is driven primarily by isoprene emission, though with the caveat that the DC-8 sampling
6 strategy did not include profiles directly over cities. While there were extensive boreal fires in
7 Alaska and northern Canada during the study period [Pfister *et al.*, 2005], because of the short
8 HCHO lifetime they did not significantly impact the column integral HCHO during the vertical
9 profiles.

10 The HCHO column is strongly correlated ($R^2 = 0.60$) with P_{HCHO} from isoprene, and not
11 with P_{HCHO} from other precursors (with the exception of monoterpenes). Even if isoprene were
12 the sole source of HCHO, the correlation between isoprene emissions and HCHO columns would
13 still be degraded by the smearing effect of horizontal transport. The observed correlation is
14 similar to that simulated by the GEOS-Chem model [Palmer *et al.*, 2003]. While the HCHO
15 column is also correlated with HCHO production from the monoterpenes α - and β -pinene ($R^2 =$
16 0.65), the highest observed P_{HCHO} from these compounds is a factor of 10 less than the satellite
17 detection limit of 0.6×10^{12} molecules $\text{cm}^{-2} \text{s}^{-1}$. The observed correlation is likely due to
18 collocation of monoterpene and isoprene emissions. It has been suggested [Kurpius and
19 Goldstein, 2003; Di Carlo *et al.*, 2004; Goldstein *et al.*, 2004; Holzinger *et al.*, 2005] that reactive
20 biogenic emissions from forests may include large amounts of unmeasured, possibly terpenoid,
21 species. The reactivity-weighted abundance of these unmeasured compounds would have to be
22 approximately 100 times greater than the sum of α - plus β -pinene to generate values of P_{HCHO}

comparable to those observed for isoprene, assuming comparable HCHO production yields. The fact that the simulated HCHO is in good agreement with the NCAR data (and is higher than the URI data), together with the fact that the distribution of HCHO columns over North America correlates with isoprene, not terpene, emission patterns [Palmer *et al.*, 2006], indicates that any inherent bias in the approach due to unmeasured reactive terpenes is small.

Figure 6 shows the relationship between observed HCHO columns and P_{HCHO} for the different precursors. Again we see that methane and the OVOCs give rise to a significant background P_{HCHO} of $\sim 1 - 1.5 \times 10^{12}$ molecules $\text{cm}^{-2} \text{s}^{-1}$, but not to variability that that would be detectable from space. When the HCHO column exceeds the fitting uncertainty by a sufficient margin to provide a useful signal to the satellite instrument, changes are driven by isoprene. We conclude that space-borne measurements of HCHO columns can reliably be used as a direct proxy for isoprene emissions over North America. This calculation provides an observational basis for previous studies, which have relied on modeled HCHO-isoprene relationships.

6. HCHO Yield from Isoprene

Using HCHO column data from space as a proxy for isoprene emission requires quantification of the relationship between the two. This has been done previously using GEOS-Chem model output [Palmer *et al.*, 2003; Palmer *et al.*, 2006] and we use here the INTEx-A vertical profiles as a test of this approach. From Equation (4), the slope of a linear regression of column HCHO (Ω_{HCHO}) vs. column isoprene (Ω_{ISOP}), normalized by the ratio of the effective loss rate constants k_{HCHO} and k_{ISOP} , represents the molar yield of HCHO production from isoprene oxidation. Figure 7a (black symbols) shows a scatterplot of modeled $k_{\text{HCHO}}\Omega_{\text{HCHO}}$ vs. $k_{\text{ISOP}}\Omega_{\text{ISOP}}$,

over the spatial domain encompassed by the continental and near-shore aircraft profiles (27.82° – 49.80° N; 59.81° – 98.96° W) and averaged over the INTEX-A timeframe. The reduced major axis slope, 1.84, is consistent with the nominal yield in Table 1 (2.3), given that the latter value assumes the high-NO_x limit and that the integrated yield is a time-dependent quantity. Figure 7b (black symbols) shows modeled Ω_{HCHO} vs. Ω_{ISOP} for the same region and time frame, with a slope of 3.99. The ratio of the slopes from the two plots (2.2) corresponds to the mean ratio $k_{\text{ISOP}}/k_{\text{HCHO}}$.

Plots of Ω_{HCHO} vs. Ω_{ISOP} calculated from concentrations measured aboard the DC-8 aircraft or simulated along the flight track during the continental and near-shore vertical profiles are shown in Figures 7b (model, red symbols) and 7c (measurements). Using the model value $k_{\text{ISOP}}/k_{\text{HCHO}} = 2.2$, which should be reliable (errors in model OH partly cancel in the ratio), the observed Ω_{HCHO} - Ω_{ISOP} slope implies an average molar HCHO yield from isoprene oxidation of 1.63 ± 0.26 , compared to the modeled value of 1.66 ± 0.27 . Uncertainties reflect the standard error of the regression. Error estimates computed using jackknife resampling are slightly higher (0.33 and 0.52 for the modeled and measured values, respectively). We conclude from the INTEX-A data that the GEOS-Chem HCHO yield from isoprene oxidation is correct to within 30%.

7. Uncertainty in the Air Mass Factor

7.1. AMF Simulation

In this section we employ the extensive mapping of HCHO over North America from the INTEX-A mission to quantify the uncertainties and bias in the AMF calculation. To do so, we calculate air mass factors separately based on measurements and based on model results, for each

1 of the DC-8 vertical profiles during INTEx-A. Assuming that the measurements perfectly
2 represent the atmosphere, the comparison statistics between the measured and modeled AMFs
3 give a measure of the corresponding error in retrieved satellite HCHO vertical columns.

4 Measured and modeled air mass factors were calculated from Equation 2 for a nadir viewing
5 geometry. Shape factors, $S(P)$, were determined using either measured or modeled HCHO mixing
6 ratios. Extrapolation of mixing ratios above and below the profile was done in the same way as
7 for the column estimates (section 4.2). Measured and modeled shape factors averaged over all the
8 continental and oceanic vertical profiles are displayed in Figure 8. The GEOS-Chem model
9 accurately captures the mean shape of the vertical profile, including the steep drop-off above the
10 continental boundary layer.

11 Scattering weights, $w(P)$, for each profile were computed using the Linearized Discrete
12 Ordinate Radiative Transfer (LIDORT) model [*Spurr et al.*, 2001], and include scattering by air
13 molecules, aerosols and clouds. Surface UV albedos are from a climatological database based on
14 GOME observations [*Koelemeijer et al.*, 2003]. Aerosol effects on the measured AMF values
15 were accounted for using local aerosol scattering and absorption measured at 10 - 60 second
16 resolution aboard the aircraft [*Clarke et al.*, 2006; *Howell et al.*, 2006]. The median single
17 scattering albedo at 346 nm during the aircraft profiles is 0.88 (0.1 – 0.9 quantiles: 0.76 – 0.97).
18 However, the aerosols encountered near the surface ($P > 800$ hPa), where the majority of the
19 aerosol (and HCHO) column resides, were predominantly scattering (median single scattering
20 albedo 0.97). The measured aerosol absorption coefficient has a large percentage of missing
21 values, which we fill in by applying the mean single-scattering albedo to the measured scattering
22 coefficient. Integrating the measured aerosol extinction over the individual vertical profiles yields

aerosol optical thicknesses (AOTs) at 346 nm ranging from 0.05 to 0.83, with a mean of 0.26 (Figure 9). The corresponding modeled AOTs computed from GEOS-Chem and used in the modeled AMF calculation range from a minimum of 0.03 to a maximum of 0.66 with a mean of 0.22 (Figure 9). A reduced major axis regression of the modeled vs. measured AOTs yields a slope of 0.73, and a coefficient of determination (R^2) of 0.41. The model reproduces the general vertical shape of the measured aerosol extinction, in particular the sharp decrease above the continental boundary layer which is similar to that observed for HCHO (Figure 8). However, the modeled extinction is biased high in the marine boundary layer and biased low in the continental boundary layer.

The impact of clouds on the measured AMFs was included using in situ cloud extinction measurements made during the vertical profiles [Clarke *et al.*, 2006], as shown in Figure 9. Only 16 of the profiles have cloud optical thicknesses greater than unity because the DC-8 flight strategy favored clear-sky profiling. For the modeled AMF, we assume that there is accurate information available regarding the cloud top height and optical thickness, since those parameters can be retrieved from satellite instruments such as GOME [Martin *et al.*, 2002a]. Here we take the cloud top and total optical thickness information from the aircraft cloud extinction data, and distribute the cloud optical thickness vertically below cloud top following Martin *et al.* [2002a] by assuming an optical thickness of 8 per 100 hPa of cloud. The cloud top height is taken as the maximum altitude above which the cloud optical thickness is greater than unity (detection limit from GOME; T.P. Kurosu, personal communication, 2005). Profiles having an integrated cloud optical thickness less than one were treated as being cloud-free for the modeled AMF calculation, but not for the measured AMF calculation.

The resulting mean vertical profiles of scattering weights $w(P)$ are shown in Figure 8 for continental and oceanic scenes. The vertical distribution reflects the increasing sensitivity of the satellite instrument with altitude, and deviates from a smooth curve due to cloud and aerosol scattering. As we see, model assumptions regarding aerosols and clouds do not incur significant error in the mean $w(P)$ profile, although this could reflect the prevalence of clear-sky scenes. A more specific assessment of the error for cloudy scenes is presented below.

Measured and modeled AMFs for the ensemble of INTEx-A vertical profiles are mapped in Figure 10 and compared in Figure 11. A reduced major axis regression of the modeled vs. measured AMF gives a slope of 0.78 and an R^2 of 0.45 (Figure 11). This includes all clear and cloudy profiles. As the overall AMF for a partly cloudy scene is given by a weighted average of the clear and cloudy values (Equation 3), we can assess the errors in AMF_{clear} and AMF_{cloud} separately using the clear and cloudy profiles, and that in the overall AMF as a function of the cloud fraction f . In what follows, AMF comparisons are given in terms of harmonic means, since the dependence of the HCHO vertical column on the slant column is defined by the inverse of the AMF. Biases in the modeled AMF are calculated as $(AMF_{\text{mod}} - AMF_{\text{meas}})/\max(AMF_{\text{mod}}, AMF_{\text{meas}})$; the AMF bias is opposite in sign to the resulting effect on the retrieved HCHO vertical column.

7.2. AMF_{clear}

For all clear-sky profiles ($N = 31$), the measured and modeled AMFs range from 0.72 – 1.69 and from 1.00 – 1.71, respectively (Figure 11, Table 2). The harmonic means (1.21 and 1.23) are identical to within one standard error. The mean bias in the modeled AMF is less than 1%; the

standard deviation of the bias, which gives a measure of the precision of the retrieval, is 17%. To the extent that the model error is random, the uncertainty in time-averaged vertical profiles of HCHO will decrease with increasing observations.

The AMF uncertainty for continental profiles under clear-sky conditions is comparable to that for the entire dataset (SD of the bias: 18%), while that for oceanic profiles is lower (SD of the bias: 10%). The mean bias in the modeled AMF is -2% (SE: 4%) over the continent, and +7% (SE: 4%) over the ocean.

7.3. AMF_{cloud}

Of the 69 aircraft profiles, 16 have cloudy skies (cloud optical thickness greater than one). Of these, only 3 have a sufficient number of HCHO and aerosol extinction measurements to compute air mass factors. In order to make the best use of the available data, and in view of the importance of determining cloud effects, we calculated cloudy AMFs by applying the 16 cloud profiles to each of the 34 vertical profiles with adequate HCHO and aerosol data. This gives 544 values of AMF_{cloud} (Figure 11, Table 2). The measured and modeled distributions of AMF_{cloud} show two distinct modes, the first at AMF values less than one and the second at values greater than one (Figure 11). This reflects the tendency of low clouds to increase the measurement sensitivity, and of high clouds to decrease the sensitivity. The mean bias in the modeled AMF_{cloud} is +46% (compared to <1% for AMF_{clear}), and the standard deviation of the bias is 39% (compared to 17% for AMF_{clear}). Uncertainty in the retrieved cloud parameters themselves is another source of error, which we do not consider explicitly here. [Koelemeijer et al., 2001], comparing two different cloud retrieval schemes, report average differences of 0.04 and 65 hPa

for cloud fraction and cloud top pressure. Comparing four cloud fraction retrievals along four GOME tracks, [Tuinder *et al.*, 2004] found the mean difference between products to range from 2-25%. Clouds are therefore the largest source of error in the AMF calculation.

7.4. AMF for Partly Cloudy Scenes

A useful parameter for the satellite retrieval is the cloud fraction above which the AMF error becomes unacceptably large. Here, we employ the 544 measured values of AMF_{cloud} to derive a measure of the AMF error as a function of the cloud fraction of the retrieval scene. The weighted average AMF was calculated from Equation (3) for cloud fractions ranging from zero to one. Figure 12 shows the bias and the standard deviation of the bias in the modeled AMF as a function of the cloud fraction of the scene. The mean bias from the 544 partly cloudy AMF calculations (solid black line in Figure 12) is 10%, 14%, 17%, and 21% at cloud fractions of 30%, 40%, 50% and 60%. The standard deviation in the bias reflects the precision in the AMF calculation, with values of 19%, 21%, 23%, and 25% at cloud fractions of 30%, 40%, 50% and 60% (red line in Figure 12). Based on this result, we recommend discarding scenes with 50% cloud coverage or more. This does not include uncertainty arising from the surface albedo, which is considered separately below.

In addition to clouds, the other important sources of model uncertainty in the AMF calculation are the shape factor, aerosols, and the surface albedo. In order to identify potential areas for improvement in the AMF calculation, the effects of these are assessed individually using sensitivity calculations described below.

7.5. Surface Albedo

Surface albedos for AMF calculations may be obtained from climatological databases derived from satellite measurements [Martin *et al.*, 2003a; Beirle *et al.*, 2004a; Boersma *et al.*, 2004; Martin *et al.*, 2004; Konovalov *et al.*, 2005; Palmer *et al.*, 2006]. The precision of the surface albedo database derived from GOME spectra is estimated at 0.02 [Koelemeijer *et al.*, 2003]. We assessed the resulting error in the HCHO air mass factor by recalculating the modeled clear-sky AMFs with the UV albedos uniformly increased and decreased by 0.02. The resulting AMF values have a mean bias of +5% in the first case, and -5% in the second. We therefore estimate the 1σ uncertainty introduced by the surface albedo at 5%.

Adding this quantity in quadrature to the standard deviation of the AMF bias calculated above as a function of cloud fraction, results in an overall 1σ uncertainty due to the AMF which increases from 15% for clear skies, to 18%, 20%, 22%, and 24% at $f = 0.2, 0.3, 0.4$, and 0.5 .

7.6. Aerosols

In order to examine the importance of aerosols for the AMF calculation, and the extent to which the GEOS-Chem model captures this effect, the measured and modeled AMFs were calculated for each vertical profile assuming aerosol-free conditions. For the purposes of this aerosol sensitivity study, we use the 19 out of 34 profiles where the aerosol absorption was measured rather than estimated. On average, the presence of aerosols increases the measured AMF by 14% relative to the aerosol-free scenario. The effect is substantially larger over the North American continent (16% increase) than over the ocean (2% increase) due to higher aerosol loadings (mean column optical thickness of 0.3 vs. 0.1). The modeled AMF using the GEOS-

Chem aerosol profile information also shows a positive sensitivity to aerosols, somewhat stronger than observations (22% over continents, 10% over the ocean).

7.7. Shape Factor

Errors introduced in the AMF due to the use of the modeled HCHO shape factor were assessed by using the measured HCHO vertical profile in the calculation of the modeled AMF. In the mean, errors in the model shape factor change the bias in the modeled AMF from +5% to -2% over the continent and from +3% to +7% over the ocean. Over the continent, the positive bias induced in the AMF by the modeled aerosol (+5%) is therefore masked by the negative bias induced by the modeled shape factor (-7%).

7.8. AMF Variability

Using CTM simulations of HCHO vertical profiles for individual scenes to calculate AMFs ensures consistency when comparing the resulting observed vertical columns to those simulated by the same CTM. For the more general purpose of displaying observed vertical columns, however, there is advantage to using a single representative HCHO profile, since this ensures that variability in the observations is real and not introduced by the model.

Overall, the modeled AMF captures 45% of the variability in the measured AMF (Figure 11). This is mostly driven by cloud scenes. The variability in the clear-sky AMF is low (relative standard deviation, $RSD_c = 0.15$) and not significantly captured by the model; tests indicate that this is primarily due to error in the HCHO shape factor. The low variability in the measured AMF_{clear} indicates that factors such as mixing height do not introduce significant variability into

the AMF. The coefficient of determination between the inverse of the measured and modeled AMFs increases with cloud fraction to $R^2(\text{AMF}_{\text{meas}}^{-1}, \text{AMF}_{\text{mod}}^{-1}) = 0.61$ at $f = 0.5$. The noise that is introduced in the retrieved columns from the modeled AMF, given by $(1 - R^2(\text{AMF}_{\text{meas}}^{-1}, \text{AMF}_{\text{mod}}^{-1})) * \text{RSD}(\text{AMF}_{\text{mod}}^{-1})$, increases from 0.12 at $f = 0$ to 0.17 at $f = 0.5$.

8. Conclusions

We used extensive aircraft vertical profiling over North America during the INTEX-A mission in summer 2004 to quantify the errors in retrieving and interpreting HCHO column data from space. By correlating the aircraft observations of HCHO columns with the column HCHO production rates inferred from concurrent VOC measurements, we showed that variability in the HCHO column over North America in summer is mainly determined by isoprene emission. For the ensemble of the INTEX-A profiles, none of the other VOCs contributed to HCHO at a level that would be detected from space, with the caveat that the DC-8 sampling strategy did not include profiles directly over cities. Satellite retrievals of HCHO columns can therefore be used reliably as a proxy for isoprene emissions over North America. In addition to providing independent constraints on emission inventories, these data offer the opportunity to examine the sensitivity of isoprene emissions to environmental drivers, assess the magnitude and implications of interannual variability in biogenic emissions [Abbot *et al.*, 2003; Palmer *et al.*, 2006], and study the effects of human influences such as logging and land-use change on emissions of isoprene.

Relating HCHO columns to isoprene emissions requires accurate knowledge of the yield of HCHO from isoprene oxidation. From correlation of measured HCHO and isoprene columns measured from the aircraft, we estimate a molar HCHO yield of 1.6 ± 0.5 . This value is

1 consistent with current chemical mechanisms used in CTMs, and in particular in the GEOS-
2 Chem CTM used in past interpretation of GOME HCHO column data. The observed correlation
3 between HCHO and isoprene columns has an R^2 of 0.60, again consistent with GEOS-Chem and
4 indicating some horizontal smearing due to the time lag between isoprene emission and HCHO
5 production.

6 The primary source of error in HCHO satellite retrievals is the air mass factor (AMF), which
7 defines the relationship between measured radiances and HCHO vertical columns. The standard
8 approach for computing the AMF is to use local vertical profile information from a CTM, and
9 we have used GEOS-Chem for this purpose in the past. Here we compared the AMFs calculated
10 from the observed vertical profiles of HCHO, aerosol extinction, and cloud extinction to those
11 calculated using GEOS-Chem model HCHO and aerosol profiles combined with the cloud
12 information one would expect to get from space (cloud top and total optical thickness). Aerosols
13 increase the AMF over North America by 16% on average and are thus important to include in
14 the AMF calculation.

15 Our analysis shows that clouds are the main source of error in the model AMF calculation.
16 The mean bias in the model AMF increases from <1% under clear-sky conditions to 17% under
17 50% cloudy conditions. The residual 1σ error (after subtraction of the mean bias) is 15% under
18 clear-sky conditions and 24% under 50% cloudy conditions. The UV surface albedo used in our
19 AMF calculation results in an AMF uncertainty of $\pm 5\%$. Combining these quantities in
20 quadrature with a fitting uncertainty of 4×10^{15} molecules cm^{-2} , we arrive at an overall 1σ
21 uncertainty in retrieved HCHO vertical columns which increases from 25% at $f=0$ to 31% at $f=$
22 0.5, for a slant column of 2×10^{16} molecules cm^{-2} . We recommend discarding retrieval scenes
23 with greater than 50% cloud cover. The fraction of the total data coverage this represents will

1 depend on the size of the satellite footprint. GOME scenes with >40% cloud cover represent
2 approximately 40% of the data coverage over North America in summer [Abbot *et al.*, 2003].
3 [Beirle *et al.*, 2004b] report that the percentage of GOME pixels with less than 10% cloud
4 coverage increases from 39% in standard forescan mode to 49% in narrow swath forescan mode.

5 In the absence of clouds, AMF variability is low (RSD = 0.15). We find that the artificial
6 variability that is introduced in HCHO column retrievals from the use of AMFs modeled using
7 the GEOS-Chem CTM is 12-17% when the cloud fraction is less than 0.5.

8 How accurately we can infer isoprene emissions from HCHO column measurements made
9 from space depends on the retrieval errors, as well as uncertainties in the HCHO yield, errors in
10 the HCHO loss rate, and uncertainties associated with converting the HCHO column at the
11 satellite overpass time to a diurnal average. Modeled HCHO yields from isoprene oxidation can
12 differ by 30% between models at a given NO_x level [Palmer *et al.*, 2006], with differences
13 highest at low NO_x. The HCHO yield calculated in the present work also has an estimated
14 uncertainty of 30%. Errors associated with the HCHO loss rate and diurnal cycle are likely to be
15 minor in comparison. The uncertainty in the HCHO production yield, combined in quadrature
16 with the retrieval errors calculated above, results in a 1 σ uncertainty in isoprene emissions
17 derived from satellite measurements of HCHO columns of 39 - 43% (again for a slant column
18 abundance of 2×10^{16} molecules cm⁻²). This level of uncertainty compares favorably with that
19 associated with extrapolating leaf and plant-level emission data [Guenther *et al.*, 2000]. The
20 overall approach therefore offers a useful and independent means of inferring surface emissions
21 of isoprene.

22 In other parts of the world, processes such as biomass burning [Thomas *et al.*, 1998; Burrows
23 *et al.*, 1999; Spichtinger *et al.*, 2004; Meyer-Arnek *et al.*, 2005] and anthropogenic emissions [Fu

et al., 2006] can also make significant and detectable contributions to column HCHO. New satellite instruments such as OMI, aboard Aura, and GOME-2, to be launched aboard the MetOp satellites, should enable mapping of biogenic, urban and biomass burning VOC emissions with much improved spatial and temporal coverage compared to GOME. The results presented here offer a foundation for future such analyses.

Acknowledgements. Financial support for this research was provided by the NASA Atmospheric Chemistry Modeling and Analysis Program, and by the NOAA Climate and Global Change Postdoctoral Fellowship Program (DBM). The authors thank Bob Yantosca, Paul Palmer, and Thomas Kurosu for their help, and the entire INTEX-A science team for their efforts.

References

- Abbot, D.S., P.I. Palmer, R.V. Martin, K.V. Chance, D.J. Jacob, and A. Guenther (2003), Seasonal and interannual variability of North American isoprene emissions as determined by formaldehyde column measurements from space, *Geophysical Research Letters*, 30 (17), 1886, doi:10.1029/2003GL017336.
- Atkinson, R. (2000), Atmospheric chemistry of VOCs and NO_x, *Atmospheric Environment*, 34 (12-14), 2063-2101.
- Atkinson, R., D.L. Baulch, R.A. Cox, J.N. Crowley, J. R. F. Hampson, R.G. Hynes, M.E. Jenkin, J.A. Kerr, M.J. Rossi, and J. Troe (2004), *Summary of Evaluated Kinetic and Photochemical Data for Atmospheric Chemistry*, IUPAC Subcommittee on Gas Kinetic Data Evaluation for Atmospheric Chemistry, Cambridge.
- Beirle, S., U. Platt, M. Wenig, and T. Wagner (2003), Weekly cycle of NO₂ by GOME measurements: a signature of anthropogenic sources, *Atmospheric Chemistry and Physics*, 3, 2225-2232.
- Beirle, S., U. Platt, R. von Glasow, M. Wenig, and T. Wagner (2004a), Estimate of nitrogen oxide emissions from shipping by satellite remote sensing, *Geophysical Research Letters*, 31, L18102, doi:10.1029/2004GL020312.
- Beirle, S., U. Platt, M. Wenig, and T. Wagner (2004b), Highly resolved global distribution of tropospheric NO₂ using GOME narrow swath mode data, *Atmospheric Chemistry and Physics*, 4, 1913-1924.
- Bey, I., D.J. Jacob, R.M. Yantosca, J.A. Logan, B.D. Field, A.M. Fiore, Q.B. Li, H.G.Y. Liu, L.J. Mickley, and M.G. Schultz (2001), Global modeling of tropospheric chemistry with assimilated meteorology: Model description and evaluation, *Journal of Geophysical Research-Atmospheres*, 106 (D19), 23073-23095.
- Blake, N.J., et al. (2003), NMHCs and halocarbons in Asian continental outflow during the Transport and Chemical Evolution over the Pacific (TRACE-P) Field Campaign:

- 1 Comparison with PEM-West B, *Journal of Geophysical Research-Atmospheres*, 108 (D20),
2 8806, doi:10.1029/2002JD003367.
- 3 Bloss, C., et al. (2005), Development of a detailed chemical mechanism (MCMv3.1) for the
4 atmospheric oxidation of aromatic hydrocarbons, *Atmospheric Chemistry and Physics*, 5,
5 641-664.
- 6 Boersma, K.F., H.J. Eskes, and E.J. Brinksma (2004), Error analysis for tropospheric NO₂
7 retrieval from space, *Journal of Geophysical Research-Atmospheres*, 109, D04311,
8 doi:10.1029/2003JD003962.
- 9 Bond, T.C., T.L. Anderson, and D. Campbell (1999), Calibration and intercomparison of filter-
10 based measurements of visible light absorption by aerosols, *Aerosol Science and Technology*,
11 30 (6), 582-600.
- 12 Burrows, J.P., et al. (1999), The global ozone monitoring experiment (GOME): Mission concept
13 and first scientific results, *Journal of the Atmospheric Sciences*, 56 (2), 151-175.
- 14 Chance, K., P.I. Palmer, R.J.D. Spurr, R.V. Martin, T.P. Kurosu, and D.J. Jacob (2000), Satellite
15 observations of formaldehyde over North America from GOME, *Geophysical Research*
16 *Letters*, 27 (21), 3461-3464.
- 17 Claeys, M., et al. (2004a), Formation of secondary organic aerosols through photooxidation of
18 isoprene, *Science*, 303 (5661), 1173-1176.
- 19 Claeys, M., W. Wang, A.C. Ion, I. Kourtchev, A. Gelencser, and W. Maenhaut (2004b),
20 Formation of secondary organic aerosols from isoprene and its gas-phase oxidation products
21 through reaction with hydrogen peroxide, *Atmospheric Environment*, 38 (25), 4093-4098.
- 22 Clarke, A.D., V. Kapustin, S.G. Howell, C.S. McNaughton, Y. Shinozuka, B. Anderson, and J.
23 Dibb (2006), Aerosol from biomass burning and regional pollution over North America
24 during INTEX-NA: Humidity response and the wavelength dependence of scattering and
25 absorption, *Journal of Geophysical Research-Atmospheres*, in preparation.
- 26 Colman, J.J., A.L. Swanson, S. Meinardi, B.C. Sive, D.R. Blake, and F.S. Rowland (2001),
27 Description of the analysis of a wide range of volatile organic compounds in whole air
28 samples collected during PEM-Tropics A and B, *Analytical Chemistry*, 73 (15), 3723-3731.
- 29 Czoschke, N.M., M. Jang, and R.M. Kamens (2003), Effect of acidic seed on biogenic secondary
30 organic aerosol growth, *Atmospheric Environment*, 37 (30), 4287-4299.
- 31 Di Carlo, P., et al. (2004), Missing OH reactivity in a forest: Evidence for unknown reactive
32 biogenic VOCs, *Science*, 304 (5671), 722-725.
- 33 Fehsenfeld, F., et al. (1992), Emissions of volatile organic compounds from vegetation and the
34 implications for atmospheric chemistry, *Global Biogeochemical Cycles*, 6 (4), 389-430.
- 35 Fiore, A.M., D.J. Jacob, I. Bey, R.M. Yantosca, B.D. Field, A.C. Fusco, and J.G. Wilkinson
36 (2002), Background ozone over the United States in summer: Origin, trend, and contribution
37 to pollution episodes, *Journal of Geophysical Research-Atmospheres*, 107 (D15),
38 10.1029/2001JD000982.
- 39 Fiore, A.M., L.W. Horowitz, D.W. Purves, H. Levy, M.J. Evans, Y.X. Wang, Q.B. Li, and R.M.
40 Yantosca (2005), Evaluating the contribution of changes in isoprene emissions to surface
41 ozone trends over the eastern United States, *Journal of Geophysical Research-Atmospheres*,
42 110, D12303, doi:10.1029/2004JD005485.
- 43 Fried, A., et al. (2003), Airborne tunable diode laser measurements of formaldehyde during
44 TRACE-P: Distributions and box model comparisons, *Journal of Geophysical Research-*
45 *Atmospheres*, 108 (D20), 8798, doi:10.1029/2003JD003451.

- 1 Fried, A., J. Walega, J. Olson, J. Crawford, G. Chen, B. Heikes, D.O. Sullivan, and H. Shen
2 (2006), The role of convection in redistributing formaldehyde to the upper troposphere over
3 North America and the North Atlantic during the summer 2004 INTEX campaign, *Journal of*
4 *Geophysical Research-Atmospheres*, in preparation.
- 5 Frost, G.J., et al. (2002), Comparisons of box model calculations and measurements of
6 formaldehyde from the 1997 North Atlantic Regional Experiment, *Journal of Geophysical*
7 *Research-Atmospheres*, 107 (D8), 4060, 10.1029/2001JD000896.
- 8 Fu, T.-M., D.J. Jacob, P.I. Palmer, and K. Chance (2006), Space-based constraints on
9 hydrocarbon emissions in East Asia, *Journal of Geophysical Research-Atmospheres*, in
10 preparation.
- 11 Fuentes, J.D., et al. (2000), Biogenic hydrocarbons in the atmospheric boundary layer: A review,
12 *Bulletin of the American Meteorological Society*, 81 (7), 1537-1575.
- 13 Goldstein, A.H., M. McKay, M.R. Kurpius, G.W. Schade, A. Lee, R. Holzinger, and R.A.
14 Rasmussen (2004), Forest thinning experiment confirms ozone deposition to forest canopy is
15 dominated by reaction with biogenic VOCs, *Geophysical Research Letters*, 31, L22106,
16 doi:10.1029/2004GL021259.
- 17 Guenther, A., et al. (1995), A global model of natural volatile organic compound emissions,
18 *Journal of Geophysical Research-Atmospheres*, 100 (D5), 8873-8892.
- 19 Guenther, A., C. Geron, T. Pierce, B. Lamb, P. Harley, and R. Fall (2000), Natural emissions of
20 non-methane volatile organic compounds, carbon monoxide, and oxides of nitrogen from
21 North America, *Atmospheric Environment*, 34 (12-14), 2205-2230.
- 22 Guenther, A., T. Karl, C. Wiedinmyer, P.I. Palmer, and C. Geron (2006), Estimates of global
23 terrestrial isoprene emissions using MEGAN (Model of Emissions of Gases and Aerosols
24 from Nature), *Atmospheric Chemistry and Physics Discussions*, 6, 107-173.
- 25 Hanst, P.L., J.W. Spence, and E.O. Edney (1980), Carbon monoxide production in
26 photooxidation of organic molecules in the air, *Atmospheric Environment*, 14 (9), 1077-1088.
- 27 Heikes, B., J. Snow, P. Egli, D. O'Sullivan, J. Crawford, J. Olson, G. Chen, D. Davis, N. Blake,
28 and D. Blake (2001), Formaldehyde over the central Pacific during PEM-Tropics B, *Journal*
29 *of Geophysical Research-Atmospheres*, 106 (D23), 32717-32731.
- 30 Hild, L., A. Richter, V. Rozanov, and J.P. Burrows (2002), Air mass factor calculations for
31 GOME measurements of lightning-produced NO₂, in *Remote Sensing of Trace Constituents*
32 *in the Lower Stratosphere, Troposphere and the Earth's Surface: Global Observations, Air*
33 *Pollution and the Atmospheric Correction*, pp. 1685-1690.
- 34 Holzinger, R., A. Lee, K.T. Paw, and A.H. Goldstein (2005), Observations of oxidation products
35 above a forest imply biogenic emissions of very reactive compounds, *Atmospheric Chemistry*
36 *and Physics*, 5, 67-75.
- 37 Howell, S., et al. (2006), On the significance of small scale aerosol features to quantitative
38 assessment of satellite validation and closure studies: MISR validations during
39 ICARTT/INTEX, *Journal of Geophysical Research-Atmospheres*, in preparation.
- 40 Hudman, R.C., et al. (2006), A multi-platform analysis of the North American reactive nitrogen
41 budget during the ICARTT summer intensive, *Journal of Geophysical Research-*
42 *Atmospheres*, in preparation.
- 43 Irie, H., et al. (2005), Evaluation of long-term tropospheric NO₂ data obtained by GOME over
44 East Asia in 1996-2002, *Geophysical Research Letters*, 32, L11810,
45 doi:10.1029/2005GL022770.

- 1 Jacob, D.J., et al. (1993), Simulation of summertime ozone over North America, *Journal of*
2 *Geophysical Research-Atmospheres*, 98 (D8), 14797-14816.
- 3 Jaeglé, L., R.V. Martin, K. Chance, L. Steinberger, T.P. Kurosu, D.J. Jacob, A.I. Modi, V.
4 Yoboue, L. Sigha-Nkamdjou, and C. Galy-Lacaux (2004), Satellite mapping of rain-induced
5 nitric oxide emissions from soils, *Journal of Geophysical Research-Atmospheres*, 109,
6 D21310, doi:10.1029/2004JD004787.
- 7 Jang, M.S., N.M. Czoschke, S. Lee, and R.M. Kamens (2002), Heterogeneous atmospheric
8 aerosol production by acid-catalyzed particle-phase reactions, *Science*, 298 (5594), 814-817.
- 9 Koelemeijer, R.B.A., and P. Stammes (1999), Effects of clouds on ozone column retrieval from
10 GOME UV measurements, *Journal of Geophysical Research-Atmospheres*, 104 (D7), 8281-
11 8294.
- 12 Koelemeijer, R.B.A., P. Stammes, J.W. Hovenier, and J.F. de Haan (2001), A fast method for
13 retrieval of cloud parameters using oxygen A band measurements from the Global Ozone
14 Monitoring Experiment, *Journal of Geophysical Research-Atmospheres*, 106 (D4), 3475-
15 3490.
- 16 Koelemeijer, R.B.A., J.F. de Haan, and P. Stammes (2003), A database of spectral surface
17 reflectivity in the range 335-772 nm derived from 5.5 years of GOME observations, *Journal*
18 *of Geophysical Research-Atmospheres*, 108 (D2), 4070, doi:10.1029/2002JD002429.
- 19 Kononov, I.B., M. Beekmann, R. Vautard, J.P. Burrows, A. Richter, H. Nuss, and N. Elansky
20 (2005), Comparison and evaluation of modelled and GOME measurement derived
21 tropospheric NO₂ columns over Western and Eastern Europe, *Atmospheric Chemistry and*
22 *Physics*, 5, 169-190.
- 23 Kurosu, T.P., K. Chance, and R.J.D. Spurr (1999), CRAG: Cloud Retrieval Algorithm for the
24 European Space Agency's Global Ozone Monitoring Experiment, in *Proceedings of the*
25 *European Symposium of Atmospheric Measurements From Space*, pp. 513 – 521, Eur. Space
26 Agency, Paris.
- 27 Kurpius, M.R., and A.H. Goldstein (2003), Gas-phase chemistry dominates O₃ loss to a forest,
28 implying a source of aerosols and hydroxyl radicals to the atmosphere, *Geophysical*
29 *Research Letters*, 30 (7), 1371, doi:10.1029/2002GL016785.
- 30 Ladstatter-Weissenmayer, A., J. Heland, R. Kormann, R. von Kuhlmann, M.G. Lawrence, J.
31 Meyer-Arnek, A. Richter, F. Wittrock, H. Ziereis, and J.P. Burrows (2003), Transport and
32 build-up of tropospheric trace gases during the MINOS campaign: comparison of GOME, in
33 situ aircraft measurements and MATCH-MPIC-data, *Atmospheric Chemistry and Physics*, 3,
34 1887-1902.
- 35 Lauer, A., M. Dameris, A. Richter, and J.P. Burrows (2002), Tropospheric NO₂ columns: A
36 comparison between model and retrieved data from GOME measurements, *Atmospheric*
37 *Chemistry and Physics*, 2, 67-78.
- 38 Lee, Y.N., et al. (1998), Atmospheric chemistry and distribution of formaldehyde and several
39 multioxygenated carbonyl compounds during the 1995 Nashville Middle Tennessee Ozone
40 Study, *Journal of Geophysical Research-Atmospheres*, 103 (D17), 22449-22462.
- 41 Leue, C., M. Wenig, T. Wagner, O. Klimm, U. Platt, and B. Jahne (2001), Quantitative analysis
42 of NO_x emissions from Global Ozone Monitoring Experiment satellite image sequences,
43 *Journal of Geophysical Research-Atmospheres*, 106 (D6), 5493-5505.
- 44 Levis, S., C. Wiedinmyer, G.B. Bonan, and A. Guenther (2003), Simulating biogenic volatile
45 organic compound emissions in the Community Climate System Model, *Journal of*
46 *Geophysical Research-Atmospheres*, 108 (D21), 4659, doi:10.1029/2002JD003203.

- 1 Levy, H. (1972), Photochemistry of the lower troposphere, *Planetary and Space Science*, 20 (6),
2 919-935.
- 3 Li, Q. (2006), Factors controlling the ozone in the middle and upper troposphere over the
4 southern United States in summer, *Journal of Geophysical Research-Atmospheres*, in
5 preparation.
- 6 Liang, Q., et al. (2006), Summertime influence of Asian pollution in the middle and upper
7 troposphere during INTEX-A, *Journal of Geophysical Research-Atmospheres*, in
8 preparation.
- 9 Lim, H.J., A.G. Carlton, and B.J. Turpin (2005), Isoprene forms secondary organic aerosol
10 through cloud processing: Model simulations, *Environmental Science & Technology*, 39 (12),
11 4441-4446.
- 12 Limbeck, A., M. Kulmala, and H. Puxbaum (2003), Secondary organic aerosol formation in the
13 atmosphere via heterogeneous reaction of gaseous isoprene on acidic particles, *Geophysical*
14 *Research Letters*, 30 (19), 1996, doi:10.1029/2003GL017738.
- 15 Lowe, D.C., and U. Schmidt (1983), Formaldehyde (HCHO) measurements in the nonurban
16 atmosphere, *Journal of Geophysical Research-Oceans and Atmospheres*, 88 (NC15), 844-
17 858.
- 18 Marquard, L.C., T. Wagner, and U. Platt (2000), Improved air mass factor concepts for scattered
19 radiation differential optical absorption spectroscopy of atmospheric species, *Journal of*
20 *Geophysical Research-Atmospheres*, 105 (D1), 1315-1327.
- 21 Martin, R.V., et al. (2002a), An improved retrieval of tropospheric nitrogen dioxide from
22 GOME, *Journal of Geophysical Research-Atmospheres*, 107 (D20), 4437,
23 doi:10.1029/2001JD001027.
- 24 Martin, R.V., et al. (2002b), Interpretation of TOMS observations of tropical tropospheric ozone
25 with a global model and in situ observations, *Journal of Geophysical Research-Atmospheres*,
26 107 (D18), 4351, doi:10.1029/2001JD001480.
- 27 Martin, R.V., D.J. Jacob, K. Chance, T.P. Kurosu, P.I. Palmer, and M.J. Evans (2003a), Global
28 inventory of nitrogen oxide emissions constrained by space-based observations of NO₂
29 columns, *Journal of Geophysical Research-Atmospheres*, 108 (D17), 4537,
30 doi:10.1029/2003JD003453.
- 31 Martin, R.V., D.J. Jacob, R.M. Yantosca, M. Chin, and P. Ginoux (2003b), Global and regional
32 decreases in tropospheric oxidants from photochemical effects of aerosols, *Journal of*
33 *Geophysical Research-Atmospheres*, 108 (D3), 4097, doi:10.1029/2002JD002622.
- 34 Martin, R.V., D.D. Parrish, T.B. Ryerson, D.K. Nicks, K. Chance, T.P. Kurosu, D.J. Jacob, E.D.
35 Sturges, A. Fried, and B.P. Wert (2004), Evaluation of GOME satellite measurements of
36 tropospheric NO₂ and HCHO using regional data from aircraft campaigns in the southeastern
37 United States, *Journal of Geophysical Research-Atmospheres*, 109, D24307,
38 doi:10.1029/2004JD004869.
- 39 Meyer-Arnek, J., A. Ladstätter-Weissenmayer, A. Richter, F. Wittrock, and J.P. Burrows (2005),
40 A study of the trace gas columns O₃, NO₂ and HCHO over Africa in September 1997,
41 *Faraday Discussions*, 130, 387-405.
- 42 Naik, V., C. Delire, and D.J. Wuebbles (2004), Sensitivity of global biogenic isoprenoid
43 emissions to climate variability and atmospheric CO₂, *Journal of Geophysical Research-*
44 *Atmospheres*, 109, D06301, doi:10.1029/2003JD004236.

- 1 Noxon, J.F., E.C. Whipple, and R.S. Hyde (1979), Stratospheric NO₂: 1. Observational method
2 and behavior at mid-latitude, *Journal of Geophysical Research-Oceans and Atmospheres*, 84
3 (NC8), 5047-5065.
- 4 Palmer, P.I., D.J. Jacob, K. Chance, R.V. Martin, R.J.D. Spurr, T.P. Kurosu, I. Bey, R. Yantosca,
5 A. Fiore, and Q.B. Li (2001), Air mass factor formulation for spectroscopic measurements
6 from satellites: Application to formaldehyde retrievals from the Global Ozone Monitoring
7 Experiment, *Journal of Geophysical Research-Atmospheres*, 106 (D13), 14539-14550.
- 8 Palmer, P.I., D.J. Jacob, A.M. Fiore, R.V. Martin, K. Chance, and T.P. Kurosu (2003), Mapping
9 isoprene emissions over North America using formaldehyde column observations from
10 space, *Journal of Geophysical Research-Atmospheres*, 108 (D6), 4180,
11 doi:10.1029/2002JD002153.
- 12 Palmer, P.I., et al. (2006), Quantifying the seasonal and interannual variability of North
13 American isoprene emissions using satellite observations of formaldehyde column, *Journal*
14 *of Geophysical Research-Atmospheres*, in press.
- 15 Park, R.J., D.J. Jacob, M. Chin, and R.V. Martin (2003), Sources of carbonaceous aerosols over
16 the United States and implications for natural visibility, *Journal of Geophysical Research-*
17 *Atmospheres*, 108 (D12), 4355, doi:10.1029/2002JD003190.
- 18 Park, R.J., D.J. Jacob, B.D. Field, R.M. Yantosca, and M. Chin (2004), Natural and
19 transboundary pollution influences on sulfate-nitrate-ammonium aerosols in the United
20 States: Implications for policy, *Journal of Geophysical Research-Atmospheres*, 109, D15204,
21 doi:10.1029/2003JD004473.
- 22 Perliski, L.M., and S. Solomon (1993), On the evaluation of air mass factors for atmospheric
23 near-ultraviolet and visible absorption spectroscopy, *Journal of Geophysical Research-*
24 *Atmospheres*, 98 (D6), 10363-10374.
- 25 Pfister, G., P.G. Hess, L.K. Emmons, J.F. Lamarque, C. Wiedinmyer, D.P. Edwards, G. Petron,
26 J.C. Gille, and G.W. Sachse (2005), Quantifying CO emissions from the 2004 Alaskan
27 wildfires using MOPITT CO data, *Geophysical Research Letters*, 32 (11), L11809,
28 doi:10.1029/2005GL022995.
- 29 Potter, C.S., S.E. Alexander, J.C. Coughlan, and S.A. Klooster (2001), Modeling biogenic
30 emissions of isoprene: Exploration of model drivers, climate control algorithms, and use of
31 global satellite observations, *Atmospheric Environment*, 35 (35), 6151-6165.
- 32 Richter, A., and J.P. Burrows (2002), Tropospheric NO₂ from GOME measurements, in *Remote*
33 *Sensing of Trace Constituents in the Lower Stratosphere, Troposphere and the Earth's*
34 *Surface: Global Observations, Air Pollution and the Atmospheric Correction*, pp. 1673-1683.
- 35 Richter, A., V. Eyring, J.P. Burrows, H. Bovensmann, A. Lauer, B. Sierk, and P.J. Crutzen
36 (2004), Satellite measurements of NO₂ from international shipping emissions, *Geophysical*
37 *Research Letters*, 31, L23110, doi:10.1029/2004GL020822.
- 38 Roller, C., A. Fried, J. Walega, P. Weibring, and F. Tittel (2006), Advances in hardware, system
39 diagnostics software, and acquisition procedures for high performance airborne tunable laser
40 measurements of formaldehyde, *Applied Physics B*, 82, 247-264.
- 41 Sander, S.P., et al. (2002), *Chemical kinetics and photochemical data for use in atmospheric*
42 *studies: Evaluation number 14*, JPL Publication 02-25, Jet Propulsion Laboratory, Pasadena.
- 43 Sanderson, M.G., C.D. Jones, W.J. Collins, C.E. Johnson, and R.G. Derwent (2003), Effect of
44 climate change on isoprene emissions and surface ozone levels, *Geophysical Research*
45 *Letters*, 30 (18), 1936, doi:10.1029/2003GL017642.

- 1 Savage, N.H., K.S. Law, J.A. Pyle, A. Richter, H. Nuss, and J.P. Burrows (2004), Using GOME
2 NO₂ satellite data to examine regional differences in TOMCAT model performance,
3 *Atmospheric Chemistry and Physics*, 4, 1895-1912.
- 4 Shepson, P.B., D.R. Hastie, H.I. Schiff, M. Polizzi, J.W. Bottenheim, K. Anlauf, G.I. Mackay,
5 and D.R. Karecki (1991), Atmospheric concentrations and temporal variations of C1-C3
6 carbonyl compounds at 2 rural sites in central Ontario, *Atmospheric Environment*, 25A (9),
7 2001-2015.
- 8 Shim, C., Y. Wang, Y. Choi, P.I. Palmer, D.S. Abbot, and K. Chance (2005), Constraining
9 global isoprene emissions with Global Ozone Monitoring Experiment (GOME)
10 formaldehyde column measurements, *Journal of Geophysical Research-Atmospheres*, 110,
11 D24301, doi:10.1029/2004JD005629.
- 12 Singh, H., et al. (2000), Distribution and fate of selected oxygenated organic species in the
13 troposphere and lower stratosphere over the Atlantic, *Journal of Geophysical Research-*
14 *Atmospheres*, 105 (D3), 3795-3805.
- 15 Singh, H.B., and P.B. Zimmerman (1992), Atmospheric distribution and sources of nonmethane
16 hydrocarbons, in *Gaseous pollutants : characterization and cycling*, edited by J.O. Nriagu,
17 pp. 177-235, Wiley, New York.
- 18 Singh, H.B., et al. (2004), Analysis of the atmospheric distribution, sources, and sinks of
19 oxygenated volatile organic chemicals based on measurements over the Pacific during
20 TRACE-P, *Journal of Geophysical Research-Atmospheres*, 109, D15S07,
21 doi:10.1029/2003JD003883.
- 22 Singh, H.B., W. Brune, J. Crawford, and D. Jacob (2006), Overview of the summer 2004
23 Intercontinental Chemical Transport Experiment-North America (INTEX-A), *Journal of*
24 *Geophysical Research-Atmospheres*, in preparation.
- 25 Spichtinger, N., R. Damoah, S. Eckhardt, C. Forster, P. James, S. Beirle, T. Marbach, T. Wagner,
26 P.C. Novelli, and A. Stohl (2004), Boreal forest fires in 1997 and 1998: A seasonal
27 comparison using transport model simulations and measurement data, *Atmospheric*
28 *Chemistry and Physics*, 4, 1857-1868.
- 29 Spurr, R.J.D., T.P. Kurosu, and K.V. Chance (2001), A linearized discrete ordinate radiative
30 transfer model for atmospheric remote-sensing retrieval, *Journal of Quantitative*
31 *Spectroscopy & Radiative Transfer*, 68 (6), 689-735.
- 32 Stohl, A., et al. (2003), Rapid intercontinental air pollution transport associated with a
33 meteorological bomb, *Atmospheric Chemistry and Physics*, 3, 969-985.
- 34 Thomas, W., E. Hegels, S. Slijkhuis, R. Spurr, and K.I. Chance (1998), Detection of biomass
35 burning combustion products in Southeast Asia from backscatter data taken by the GOME
36 spectrometer, *Geophysical Research Letters*, 25 (9), 1317-1320.
- 37 Tuinder, O.N.E., R. de Winter-Sorkin, and P.J.H. Builtjes (2004), Retrieval methods of effective
38 cloud cover from the GOME instrument: An intercomparison, *Atmospheric Chemistry and*
39 *Physics*, 4, 255-273.
- 40 Turquety, S., et al. (2006), Inventory of boreal fire emissions for North America: importance of
41 peat burning and pyro-convective injection, *Journal of Geophysical Research-Atmospheres*,
42 in preparation.
- 43 van Donkelaar, A., R.V. Martin, R.J. Park, C.L. Heald, T.-M. Fu, A. Guenther, and H. Liou
44 (2006), Evaluation of processes for secondary organic aerosol production using surface
45 observations in the United States, *Geophysical Research Letters*, in preparation.

- 1 Velders, G.J.M., C. Granier, R.W. Portmann, K. Pfeilsticker, M. Wenig, T. Wagner, U. Platt, A.
2 Richter, and J.P. Burrows (2001), Global tropospheric NO₂ column distributions: Comparing
3 three-dimensional model calculations with GOME measurements, *Journal of Geophysical*
4 *Research-Atmospheres*, 106 (D12), 12643-12660.
- 5 Virkkula, A., N.C. Ahlquist, D.S. Covert, W.P. Arnott, P.J. Sheridan, P.K. Quinn, and D.J.
6 Coffman (2005), Modification, calibration and a field test of an instrument for measuring
7 light absorption by particles, *Aerosol Science and Technology*, 39 (1), 68-83.
- 8 Wagner, V., R. von Glasow, H. Fischer, and P.J. Crutzen (2002), Are CH₂O measurements in
9 the marine boundary layer suitable for testing the current understanding of CH₄
10 photooxidation?: A model study, *Journal of Geophysical Research-Atmospheres*, 107 (D3),
11 10.1029/2001JD000722.
- 12 Wang, K.Y., and D.E. Shallcross (2000), Modelling terrestrial biogenic isoprene fluxes and their
13 potential impact on global chemical species using a coupled LSM-CTM model, *Atmospheric*
14 *Environment*, 34 (18), 2909-2925.
- 15 Wert, B.P., A. Fried, S. Rauenbuehler, J. Walega, and B. Henry (2003), Design and performance
16 of a tunable diode laser absorption spectrometer for airborne formaldehyde measurements,
17 *Journal of Geophysical Research-Atmospheres*, 108 (D12), 4350,
18 doi:10.1029/2002JD002872.
- 19 Xiao, Y.P., D.J. Jacob, J.S. Wang, J.A. Logan, P.I. Palmer, P. Suntharalingam, R.M. Yantosca,
20 G.W. Sachse, D.R. Blake, and D.G. Streets (2004), Constraints on Asian and European
21 sources of methane from CH₄-C₂H₆-CO correlations in Asian outflow, *Journal of*
22 *Geophysical Research-Atmospheres*, 109, D15S16, doi:10.1029/2003JD004475.
- 23 Zhang, R.Y., I. Suh, J. Zhao, D. Zhang, E.C. Fortner, X.X. Tie, L.T. Molina, and M.J. Molina
24 (2004), Atmospheric new particle formation enhanced by organic acids, *Science*, 304 (5676),
25 1487-1490.
- 26 Zimmerman, P.R., R.B. Chatfield, J. Fishman, P.J. Crutzen, and P.L. Hanst (1978), Estimates on
27 production of CO and H₂ from oxidation of hydrocarbon emissions from vegetation,
28 *Geophysical Research Letters*, 5 (8), 679-682.

Table 1. Formaldehyde Production Yields

Species	Molar HCHO Yield ^a
Biogenics	
Isoprene	2.3
Alpha-pinene	1.9 ^b
Beta-pinene	1.7 ^b
Alkanes	
Methane	1.0
Ethane	1.1
Propane	0.6
≥ C4 Alkanes	2.0
Alkenes	
Ethene	1.8
≥ C3 Alkenes	2.0
Aromatics	
Toluene	1.2 ^b
m-Xylene	2.1 ^b
p-Xylene	2.0 ^b
o-Xylene	2.2 ^b
Ethylbenzene	2.1 ^c
C9 Aromatics	2.3 ^c
Oxygenated VOCs (OVOCs)	
Acetone	2.0
Methanol	1.0
Ethanol	1.0
Acetaldehyde	1.0

^a Yields are from the GEOS-Chem chemical mechanism (<http://www-as.harvard.edu/chemistry/trop/geos/index.html>) except where noted. See text for details. ^b From MCMv3.1 [Bloss *et al.*, 2005; Palmer *et al.*, 2006]. ^c Estimated assuming the same per-carbon yield as m-xylene.

Table 2. AMF Comparison Statistics^a

		N	AMF		Model Bias (%)	
			Harmonic Mean	SD	Mean	SD
AMF _{clear}	<u>All Profiles</u>					
	Measured	31	1.21	0.22	-	-
	Modeled	31	1.23	0.19	0%	17%
	<u>Continental & Nearshore Profiles</u>					
	Measured	24	1.18	0.24	-	-
	Modeled	24	1.18	0.16	-2%	18%
	<u>Oceanic profiles</u>					
	Measured	7	1.34	0.05	-	-
	Modeled	7	1.43	0.16	+7%	10%
AMF _{cloud}	Measured	544 ^b	0.13 ^c	0.75	-	-
	Modeled	544 ^b	0.44 ^c	1.08	+46%	39%

^a Measured and modeled AMFs calculated from in situ measurements and chemical transport model results for each of the DC-8 vertical profiles during INTEx-A. ^b For each of the 34 vertical profiles with adequate data coverage, values of AMF_{cloud} were calculated using all of the 16 cloud profiles encountered during the entire study. ^c The harmonic mean for AMF_{cloud} is skewed by values close to zero. The median measured and modeled values are 0.35 and 0.76, respectively.

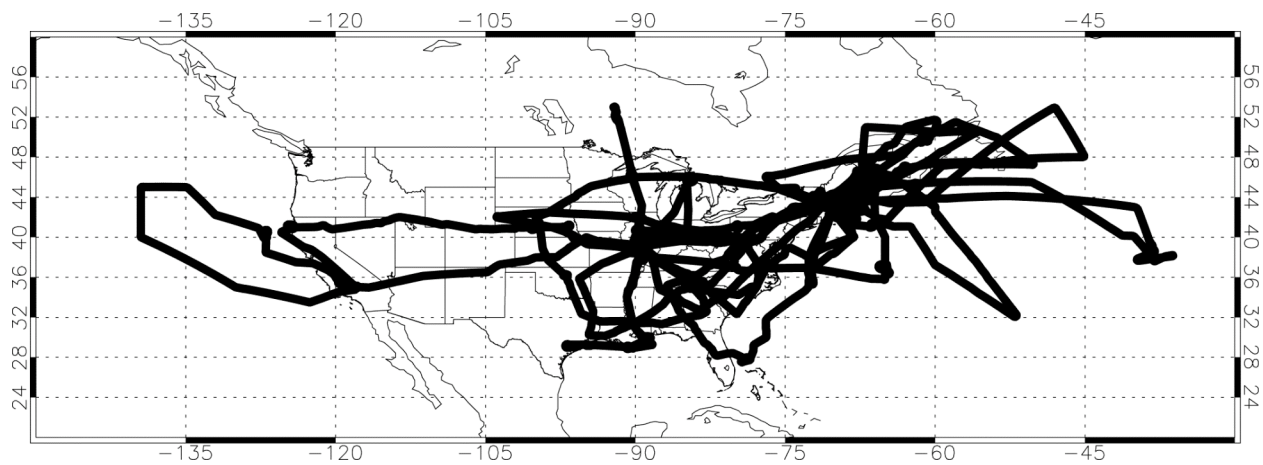


Figure 1. DC-8 flight tracks during INTEX-A.

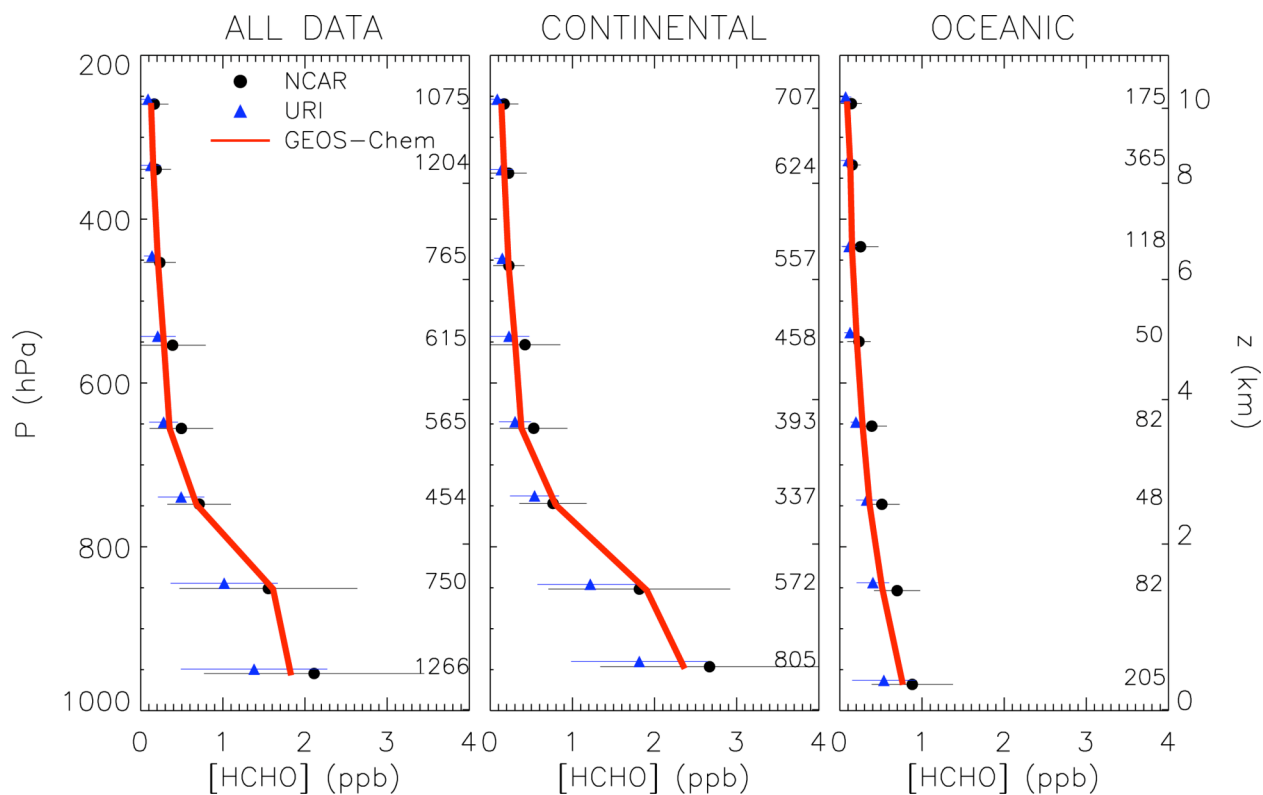


Figure 2. Mean simulated (lines) and observed (symbols) HCHO vertical distributions during INTEx-A, calculated for 100 hPa vertical bins. Error bars represent observed standard deviations (the numbers of points are indicated on the right). The vertical coordinates for the URI observations are offset slightly for visibility. Here and elsewhere, the model is sampled along the flight tracks and for the time of the measurements.

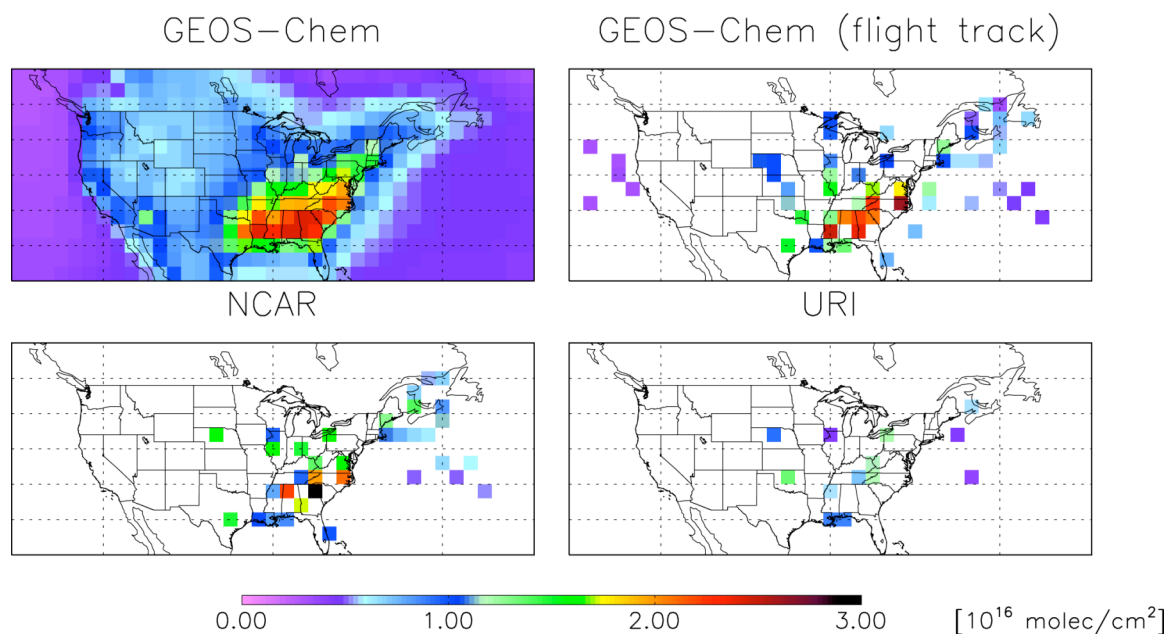


Figure 3. Atmospheric HCHO columns over North America. The top left panel shows GEOS-Chem simulated columns averaged over the INTEX-A period (July 1 – August 15, 2004). The other three panels show HCHO columns computed from HCHO mixing ratios measured (NCAR and URI) and simulated along the flight track during the DC-8 vertical profiles.

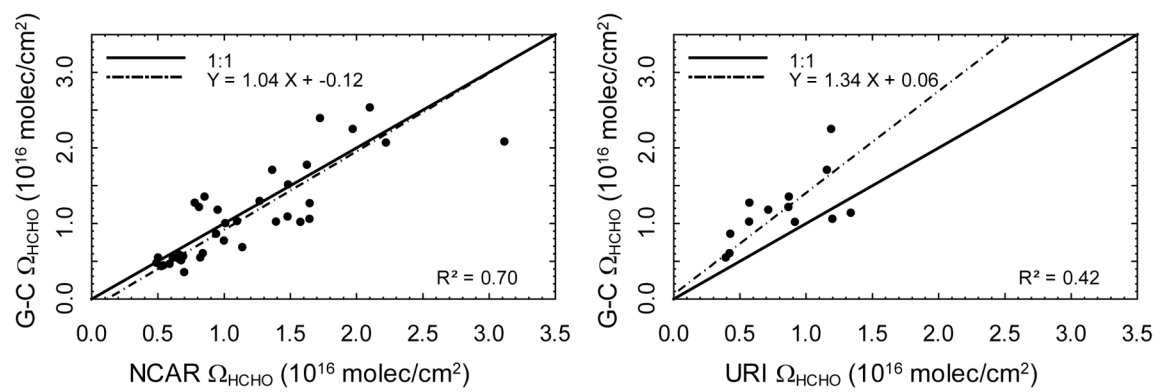


Figure 4. Scatterplots and reduced major axis regression of simulated (GEOS-Chem, G-C) vs. observed HCHO columns during INTEX-A.

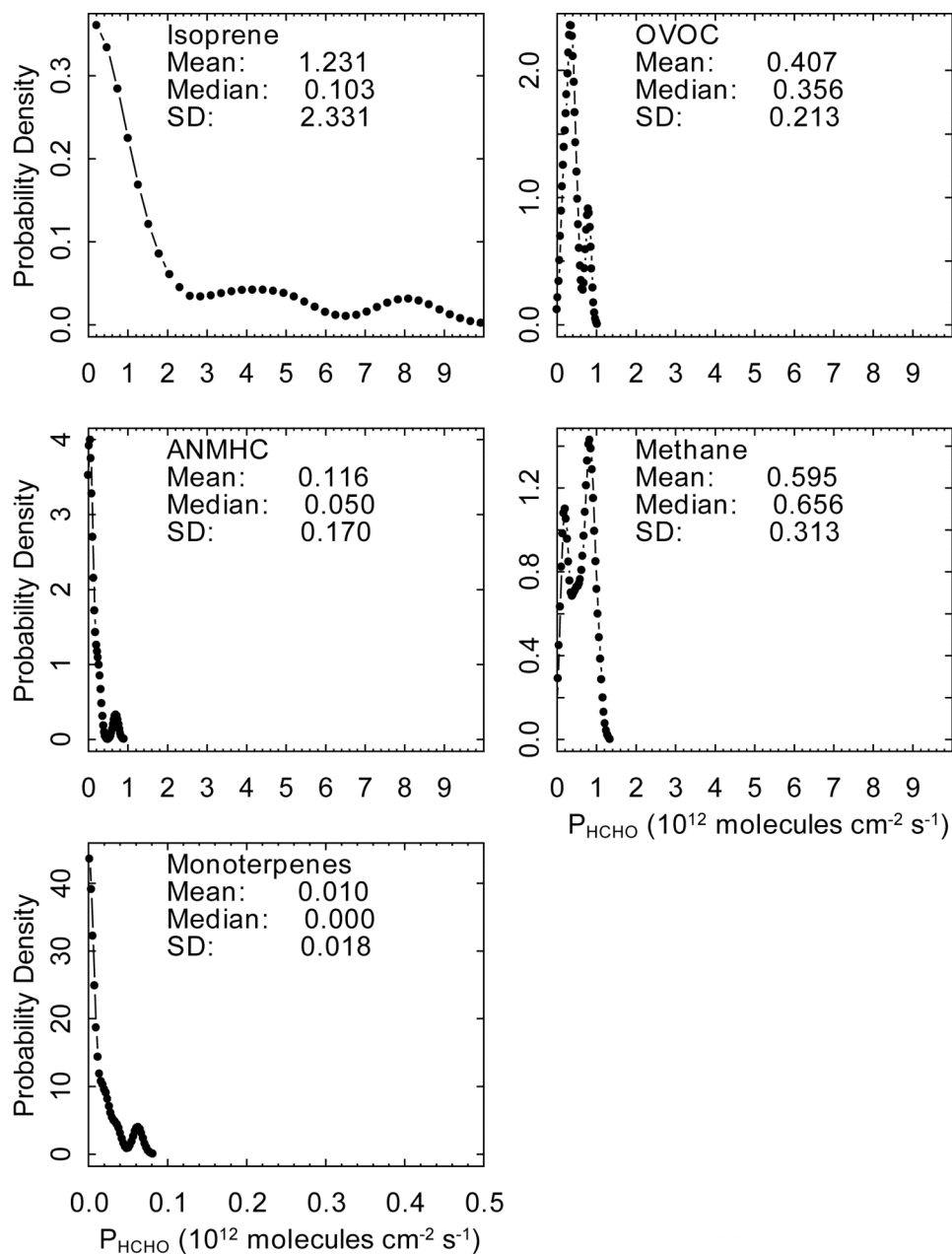


Figure 5. Probability density function of HCHO column production rates from different measured VOCs during INTEx-A vertical profiles: isoprene, oxygenated volatile organic compounds (OVOCs), anthropogenic non-methane hydrocarbons (ANMHCs), methane, and monoterpenes. The dominant OVOCs for HCHO production are methanol and acetaldehyde, while the dominant ANMHCs are ethane, butane, and isopentane. **Note the different x-axis scale in the fifth panel.**

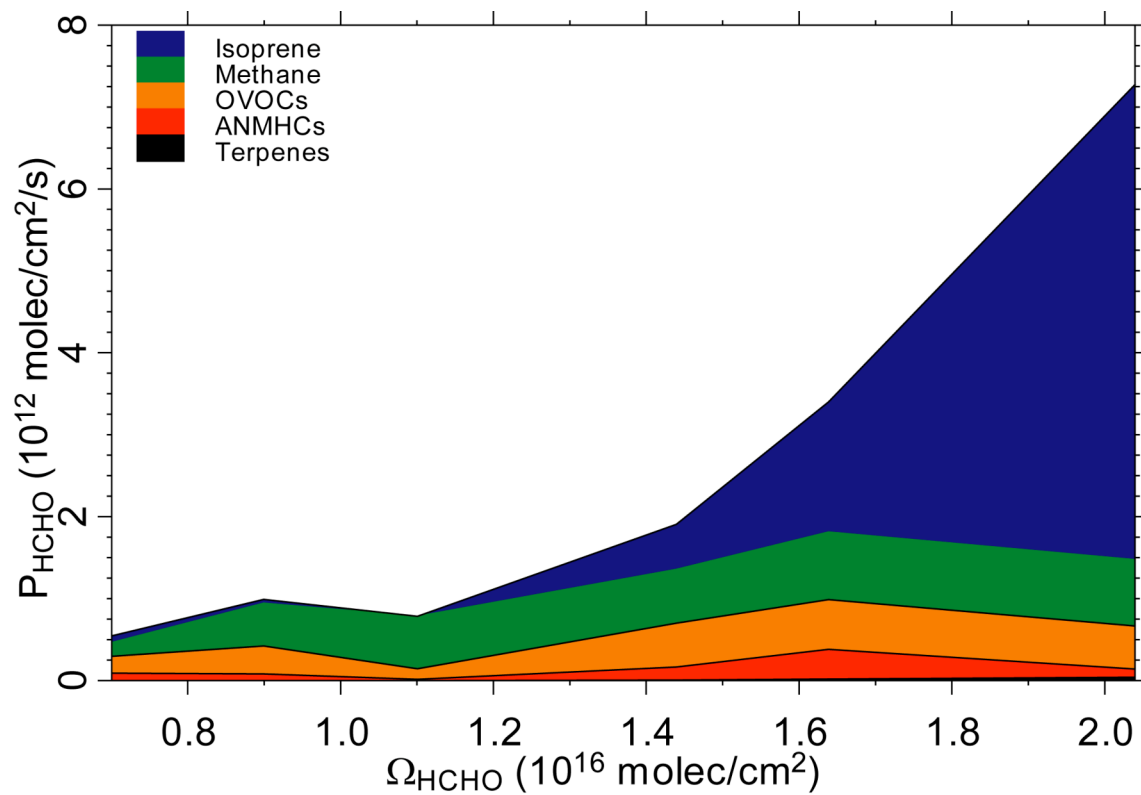


Figure 6. Stack plot showing the relationship between measured HCHO column (Ω_{HCHO}) and HCHO production rate (P_{HCHO}) from different precursors. Isoprene is the dominant source of Ω_{HCHO} variability.

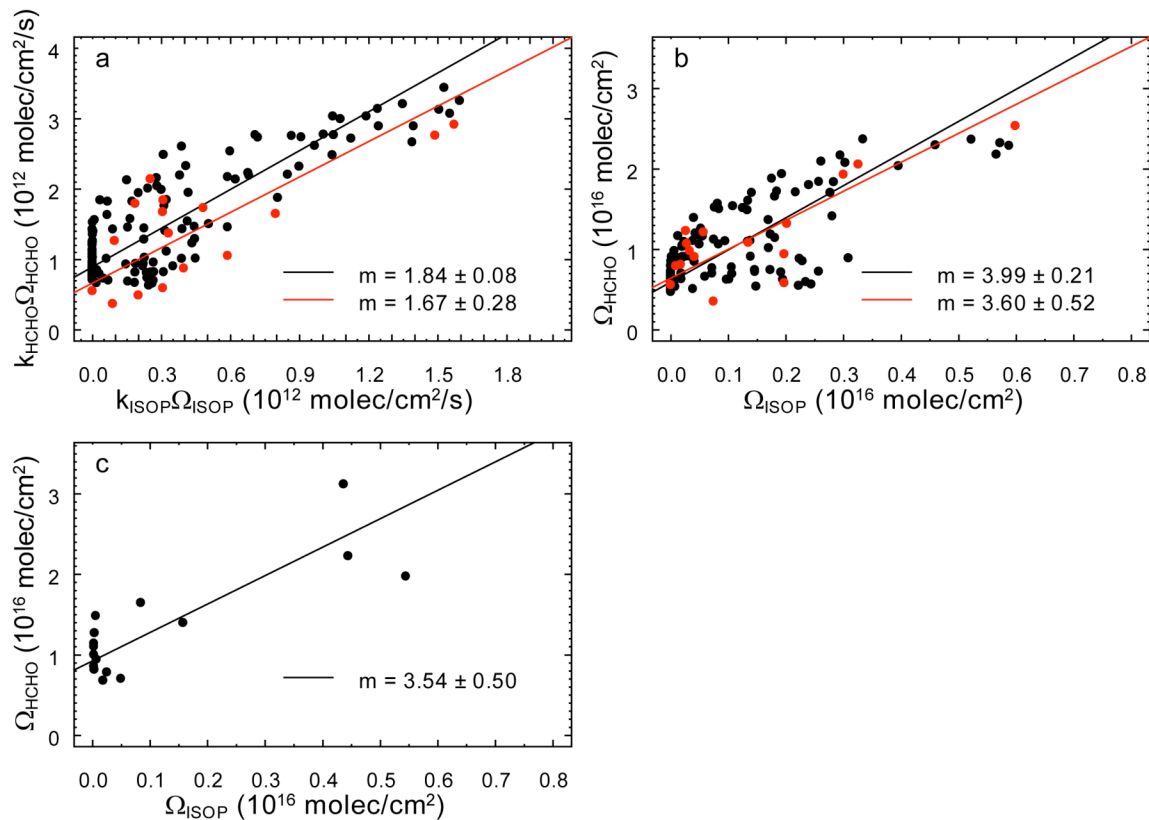


Figure 7. Simulated (panels a, b) and observed (panel c) relationships between HCHO and isoprene columns. Panel (a) shows modeled $k_{\text{HCHO}}\Omega_{\text{HCHO}}$ vs. $k_{\text{ISOP}}\Omega_{\text{ISOP}}$ averaged over the INTEx-A spatial and temporal domain (black), and for the locations and times corresponding to the DC-8 vertical profiles (red). Panel (b) shows modeled Ω_{HCHO} vs. Ω_{ISOP} with the same color scheme. Panel (c) shows Ω_{HCHO} vs. Ω_{ISOP} calculated from concentrations measured aboard the aircraft during the profiles. The observed $\Omega_{\text{HCHO}} - \Omega_{\text{ISOP}}$ slope indicates an average molar HCHO yield from isoprene oxidation of 1.6.

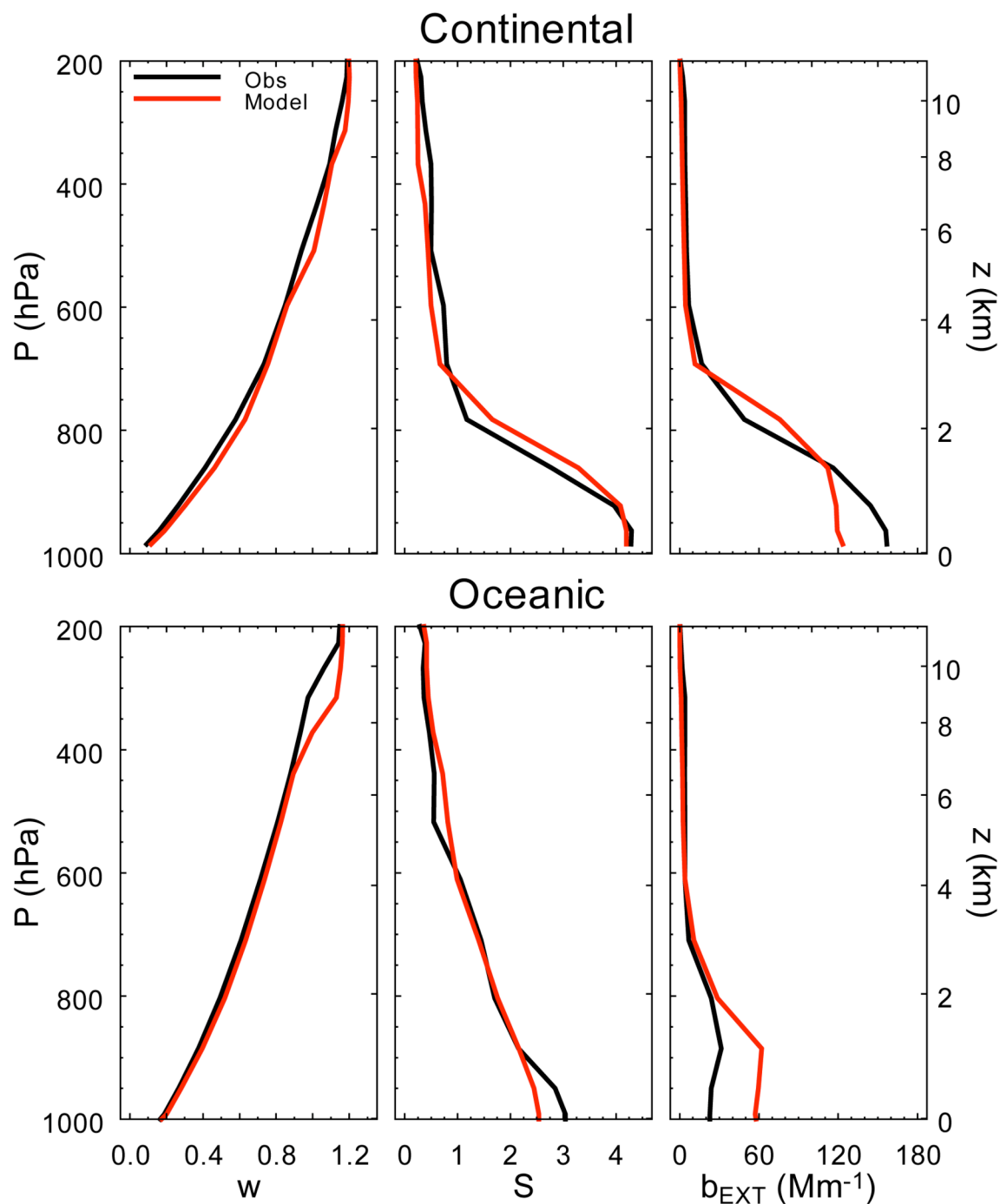


Figure 8. Measured (black) and modeled (red) vertical profiles of satellite instrument sensitivity (scattering weights, w), normalized HCHO concentration (shape factor, S), and aerosol extinction (b_{EXT} , Mm $^{-1}$), averaged over the DC-8 continental and oceanic vertical profiles during INTEx-A.

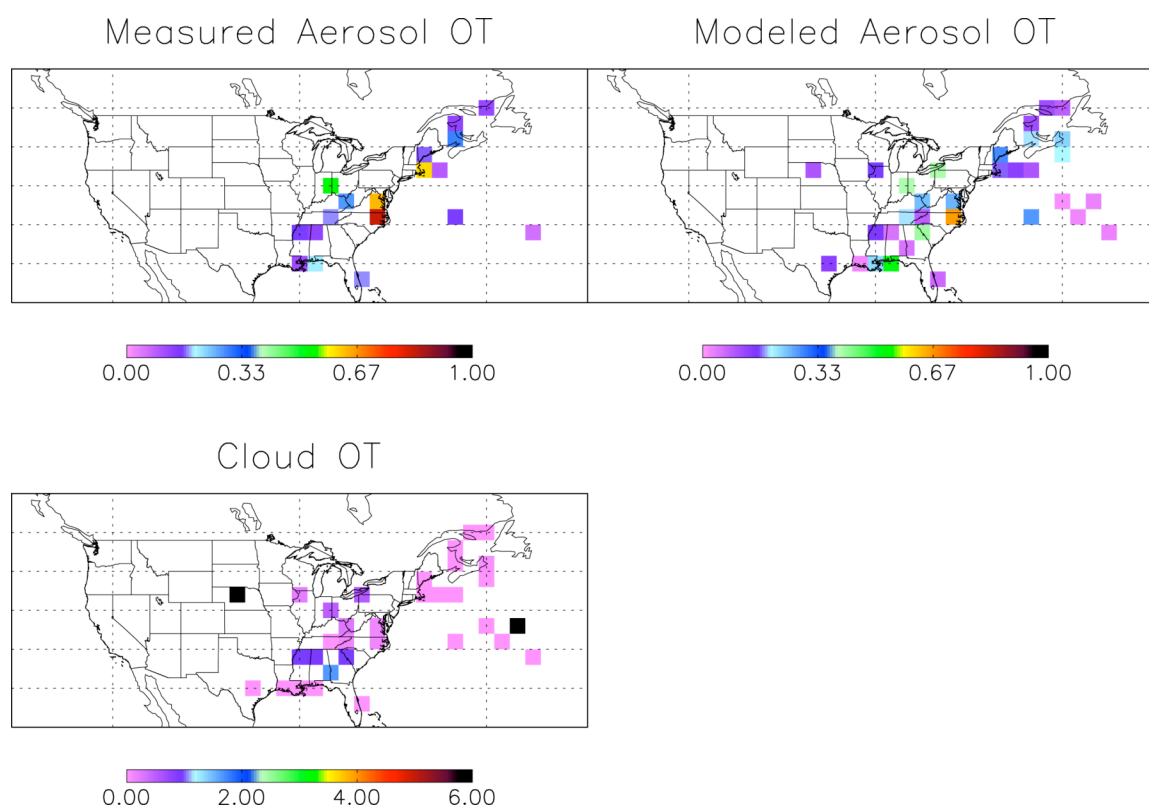


Figure 9. Measured and modeled column aerosol optical thickness, and measured cloud optical thickness, for the INTEX-A vertical profiles.

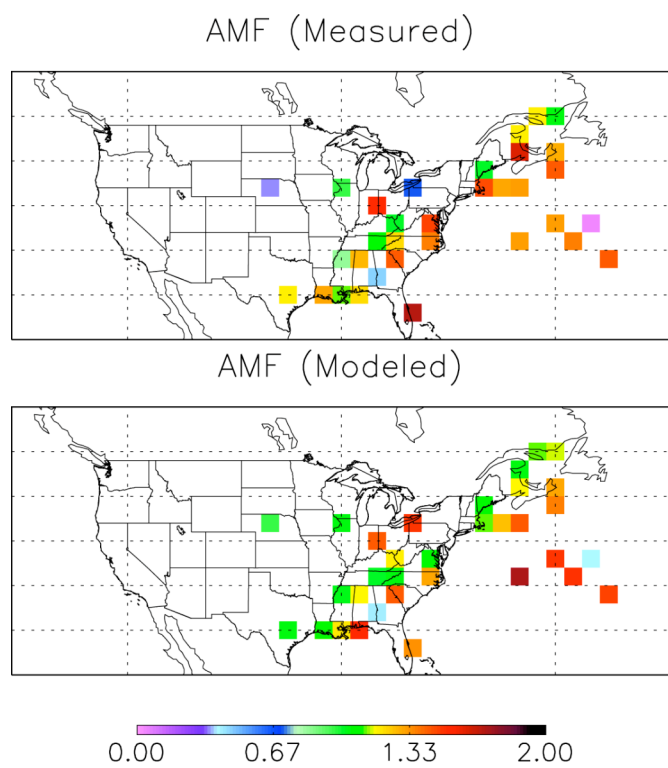


Figure 10. Measured and modeled HCHO air mass factors for the DC-8 vertical profiles during INTEX-A.

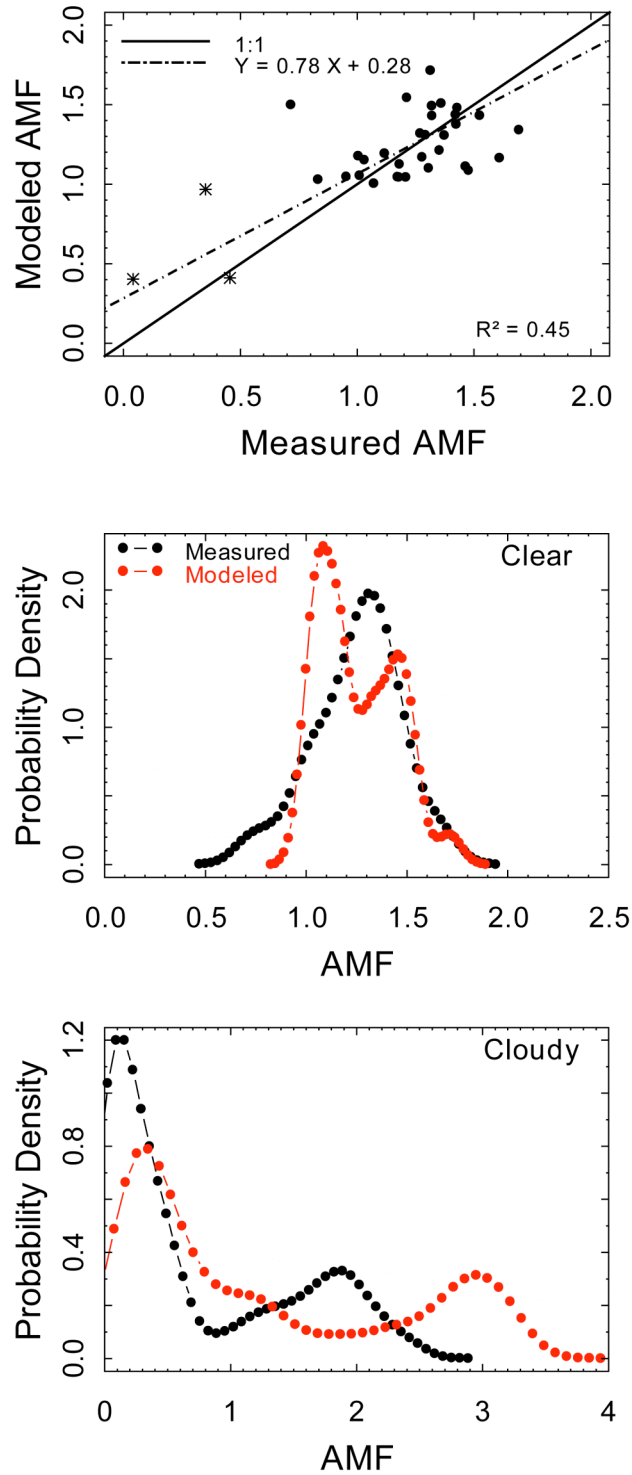


Figure 11. Top panel: scatterplot of modeled vs. measured air mass factors computed for the DC-8 vertical profiles. Clear-sky and cloudy profiles are represented by points and asterisks, respectively. The bottom two panels show probability density functions of AMF_{clear} and AMF_{cloud} . The pdf of AMF_{cloud} is based on 544 data points as described in the text.

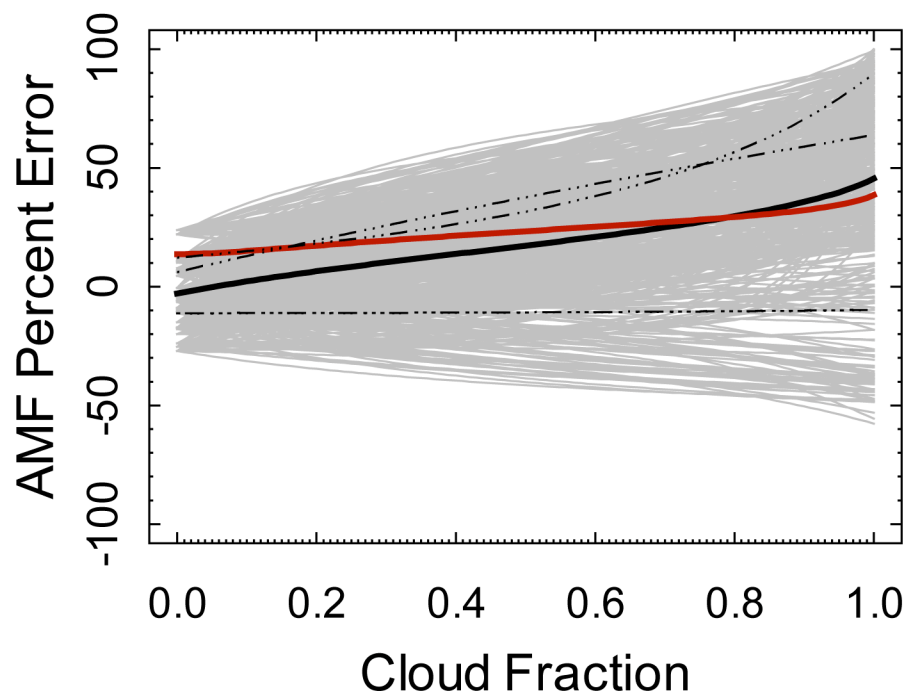


Figure 12. Error in the modeled AMF as a function of the cloud fraction. Black dot-dash lines show data for the 3 actual INTEX-A profiles having integrated cloud optical thickness greater than unity together with sufficient HCHO and aerosol data coverage. The grey lines show the errors for the 544 profiles sampled as described in the text. The solid black line shows the mean bias for these 544 calculations, and the red line shows the standard deviation in the bias.